

ON CANONICAL TRIANGULATIONS OF ONCE-PUNCTURED TORUS BUNDLES AND TWO-BRIDGE LINK COMPLEMENTS

FRANÇOIS GUÉRITAUD
WITH AN APPENDIX BY DAVID FUTER

ABSTRACT. We prove the hyperbolization theorem for punctured-torus bundles and two-bridge links by decomposing them into ideal tetrahedra which are then given hyperbolic structures.

À la mémoire de Pierre Philipps.

1. INTRODUCTION

Let $T := (\mathbb{R}^2 \setminus \mathbb{Z}^2)/\mathbb{Z}^2$ be the once-punctured torus endowed with its differential structure and an orientation. The group G of isotopy classes of orientation-preserving diffeomorphisms $\varphi : T \rightarrow T$ (or mapping class group of T) is identified as $G \simeq SL_2(\mathbb{Z})$, so such a map φ has well-defined eigenvalues in \mathbb{C} . For $[\varphi]$ in G , define the *punctured-torus bundle*

$$V_\varphi := T \times [0, 1] / \sim$$

where \sim identifies $(x, 0)$ with $(\varphi(x), 1)$ for all x in T . Then V_φ is a differentiable oriented 3-manifold, well-defined up to diffeomorphism. Thurston's Hyperbolization Theorem [Ot] implies as a very special case

Theorem 1. *If φ has two distinct real eigenvalues, the punctured-torus bundle V_φ admits a finite-volume, complete hyperbolic metric.*

The aim of this paper is to prove Theorem 1 by elementary and, to some extent, constructive arguments. The strategy is to exhibit a canonical, geodesic triangulation \mathcal{H} of V_φ into ideal tetrahedra (hyperbolic tetrahedra whose vertices are at infinity).

Combinatorially, \mathcal{H} (sometimes called the Floyd-Hatcher or monodromy triangulation) is found by expressing a certain conjugate of $\pm\varphi$ as a product of positive transvection matrices. Once such combinatorial data for a triangulation is given, the problem of making it hyperbolic lends itself to two approaches. One is complex, explicit and “local” : cross-ratio computations, particular hyperbolic isometries, etc (see e.g. [NZ]). The other one, first described by Rivin, Casson and Colin de Verdière [Ri, Co], is real-analytic and “global” : in order to make the structure complete, one kills its monodromy by maximizing the total hyperbolic volume (but combinatorial obstructions might arise). In the case of V_φ , the combinatorial structure of \mathcal{H} is sufficiently well-understood to allow a nice interplay between the two approaches, yielding useful “medium-range” results (Section 8). The philosophy of such results is that if the structure with maximal volume is non-complete, it should still be complete at “most” places, enabling us to make geometric statements.

Date: 17th June 2019.

Lackenby [La], assuming the existence of the hyperbolic metric, proved by a normal surface argument that the “combinatorially canonical” triangulation \mathcal{H} must also be “geometrically canonical”, i.e. topologically dual to the Ford-Voronoi domain of V_φ . In [Gu], we will apply the methods of the present paper to prove a stronger version of Lackenby’s result. Other references closely related to this subject include the beautiful article [ASWY], which builds on the work of Jørgensen, and the examples compiled in [AH], [He] and [Ko].

The converse of Theorem 1 is true. If the trace τ of the monodromy map φ is in $\{-1, 0, 1\}$, then $[\varphi]$ has finite order and V_φ is Seifert fibered. If $\tau = \pm 2$, then φ preserves a nontrivial simple closed curve γ (parallel to a rational eigenvector) in the punctured torus, and γ defines an incompressible torus or Klein bottle in V_φ . In any case we get a topological obstruction to the existence of the hyperbolic metric.

An attempt at self-containedness will be made in proving Theorem 1. The proof will deal primarily with the case where the eigenvalues of φ are positive. The other case is only a minor variant (in particular, $V_{-\varphi}$ can be obtained by ungluing the metric tetrahedra of V_φ and regluing them in a slightly different way).

Section 2 is standard and recalls the classification of conjugacy classes in $SL_2(\mathbb{Z})$ in order to define the triangulation \mathcal{H} . The latter is studied in greater detail in Sections 3 and 4. Positive angles for \mathcal{H} (a “linear hyperbolic structure”) are provided in Section 5. Section 6 explains the role played by hyperbolic volume maximization, allowing to deal with the easy cases in Section 7. Section 8 presents the essential geometric lemma for the final attack, carried out in Section 9. Section 10 is devoted to a numerical example. In Section 11, we quickly recall the connection between once-punctured tori and four-times-punctured spheres. In the Appendix, David Futer builds on that connection to prove an analogue of Theorem 1 for the complements of two-bridge links.

The symbol “=” is preceded (resp. followed) by a colon ($:=$, resp. $=:$) when the equality serves as a definition for its left (resp. right) member.

I would like to thank Francis Bonahon and Frédéric Paulin for numerous insights and the great improvements this paper owes to them. Exciting discussions with David Futer and with Makoto Sakuma also gave invaluable input. This paper reached its final form during a stay at the Institut Bernoulli (EPFL, Lausanne) for whose kind hospitality I express my deep gratitude. This work was partially supported by NSF grant DMS-0103511.

2. CONJUGACY CLASSES IN $SL_2(\mathbb{Z})$ AND THE FAREY TESSELLATION

Proposition 2. *Let φ be an element of $SL_2(\mathbb{Z})$ with two distinct eigenvalues in \mathbb{R}_+^* . Then the conjugacy class of φ in $SL_2(\mathbb{Z})$ contains an element of the form*

$$A\varphi A^{-1} = \begin{pmatrix} 1 & a_1 \\ 0 & 1 \end{pmatrix} \begin{pmatrix} 1 & 0 \\ b_1 & 1 \end{pmatrix} \begin{pmatrix} 1 & a_2 \\ 0 & 1 \end{pmatrix} \begin{pmatrix} 1 & 0 \\ b_2 & 1 \end{pmatrix} \cdots \begin{pmatrix} 1 & a_n \\ 0 & 1 \end{pmatrix} \begin{pmatrix} 1 & 0 \\ b_n & 1 \end{pmatrix}$$

where $n > 0$ and the a_i and b_i are positive integers. Moreover, the right hand side is unique up to cyclic permutation of the factors $\begin{pmatrix} 1 & a_i \\ 0 & 1 \end{pmatrix} \begin{pmatrix} 1 & 0 \\ b_i & 1 \end{pmatrix}$. Conversely, any non-empty product of such factors is an element of $SL_2(\mathbb{Z})$ with two distinct eigenvalues in \mathbb{R}_+^* . \square

We sketch a proof of this popular fact, mainly in order to introduce the *cyclic word* Ω associated to φ . The converse implication is easy (just check that the trace is larger than 2), so we focus on the direct statement.

Consider the upper half-plane model of the hyperbolic plane \mathbb{H}^2 , endowed with the Farey tessellation F (the ideal triangle 01∞ iteratedly reflected in its sides). We identify $PSL_2(\mathbb{R})$ with the group of isometries of \mathbb{H}^2 via the isomorphism Ψ defined by

$$\Psi \begin{pmatrix} a & b \\ c & d \end{pmatrix} : z \mapsto \frac{dz + c}{bz + a}.$$

(Under this slightly unusual convention, the slopes of the eigenvectors of M are the fixed points of $\Psi(M)$, rather than their inverses as would normally be the case). It is known that the group of orientation-preserving isometries of \mathbb{H}^2 preserving F is thus identified with $PSL_2(\mathbb{Z})$.

Let D be the oriented hyperbolic line running from the repulsive fixed point of $\pm\varphi$ to the attractive one. Then D crosses infinitely many Farey triangles $(\dots t_{-1}, t_0, t_1, t_2, \dots)$ of F . We can formally write down a bi-infinite word

$$\Omega = \dots LRRRLLR \dots$$

where the k -th letter is R (resp. L) if D exits t_k to the Right (resp. Left) of where it enters. We will also say that D *makes a Right* (resp. *Left*) at t_k . The word Ω contains at least one R and one L , because the ends of D are distinct. The image of t_0 under φ is a certain t_m ($m > 1$), and Ω is periodic of period m .

Next, define the standard transvection matrices

$$R := \begin{pmatrix} 1 & 1 \\ 0 & 1 \end{pmatrix} \quad ; \quad L := \begin{pmatrix} 1 & 0 \\ 1 & 1 \end{pmatrix}.$$

These are parabolic transformations of \mathbb{H}^2 whose respective fixed points are 0 and ∞ . Let M be any subword of Ω of length m : we see M as a product of standard transvection matrices, and therefore as an element of $SL_2(\mathbb{Z})$. By studying the actions of R and L on F , it is then easy to see that φ and M are conjugates in $PSL_2(\mathbb{Z})$, and therefore in $SL_2(\mathbb{Z})$ since both have positive trace. This proves the existence statement for the (a_i, b_i) .

Uniqueness is checked as follows: on one hand, if φ and φ' are conjugates, there is an element of $PSL_2(\mathbb{Z})$ (preserving F) that brings their axes on one another, so they define the same word Ω up to translation. On the other hand, looking at the actions of R and L on \mathbb{H}^2 , one sees that a product of standard transvection matrices (as in the statement of Proposition 2) will define the word $\Omega = R^{a_1} L^{b_1} \dots R^{a_n} L^{b_n}$, concatenated infinitely many times with itself.

In the language of Proposition 2, the sequence $(a_1, b_1, \dots, a_n, b_n)$ can be shown to be (a positive power of) the period of the continued fraction expansion of the slope of the expanding eigenvector of φ . The word Ω will be seen either as infinite periodic, or as finite cyclic, depending on the context.

3. THE CANONICAL TRIANGULATION

3.1. Diagonal exchanges. There is another well-known interpretation of the Farey tessellation F of the hyperbolic plane \mathbb{H}^2 . Under the canonical identification $H_1(T, \mathbb{Z}) \simeq \mathbb{Z}^2$, where T is the punctured torus defined in the Introduction, each rational number in the boundary $\widehat{\mathbb{R}} = \mathbb{R} \cup \{\infty\}$ of \mathbb{H}^2 can be seen as a *slope*, i.e. a

proper isotopy class of properly embedded lines in T , going from the puncture to itself. The action of $SL_2(\mathbb{Z})$ on $\widehat{\mathbb{Q}}$ coincides with the action of the mapping class group G of T on rational slopes. The edges of the Farey tessellation F connect exactly the pairs of rational numbers whose corresponding curves in T can be homotoped off each other (away from the puncture). The faces of F , having three edges, correspond exactly to the isotopy classes of *ideal triangulations* of T : any such triangulation has one vertex (the puncture), three edges, and two triangles (which meet along each edge). As one crosses from a face of F to one of its neighbors, exactly one vertex gets replaced, which in the corresponding triangulations of T means that exactly one edge is changed. Inspection shows that the triangulation must be undergoing a *diagonal exchange*: erase one edge e , thus liberating a quadrilateral space Q of which e was a diagonal, then insert back the other diagonal.

3.2. Tetrahedra. As before, let φ be an element of $SL_2(\mathbb{Z})$ with two distinct eigenvalues in \mathbb{R}_+^* . In the proof of Proposition 2, we introduced the triangles t_0, t_1, \dots crossed by the axis D of φ . In view of the above, this yields a non-backtracking path of diagonal exchanges between some triangulation (associated to t_0) and its push-forward by φ (associated to t_m).

More precisely, when the oriented line D crosses an edge e of the Farey tessellation, e comes with a transverse orientation. So we can define the *top* (resp. *bottom*) triangulation $\tau_+(e)$ (resp. $\tau_-(e)$) of the punctured torus T as being the one associated with the Farey triangle crossed just after (resp. before) the edge e . A diagonal exchange separates the triangulations $\tau_-(e)$ and $\tau_+(e)$. An ideal tetrahedron is by definition a space diffeomorphic to an ideal hyperbolic tetrahedron (topologically it is a compact tetrahedron with its vertices removed). We can immerse such an ideal tetrahedron $\Delta(e)$ in $T \times \mathbb{R}$: the boundary of the immersed $\Delta(e)$ is made up of two *pleated surfaces* (top and bottom) homotopic to T and triangulated according to $\tau_+(e)$ and $\tau_-(e)$ respectively (Figure 1). The immersion is an embedding on the interior of $\Delta(e)$, but two pairs of opposite edges undergo identifications.

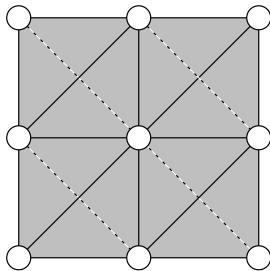


FIGURE 1. Four copies of $\Delta(e)$ in the cover $(\mathbb{R}^2 \setminus \mathbb{Z}^2) \times \mathbb{R}$ of $T \times \mathbb{R}$.

Next, if D crosses the Farey edges e_i, e_{i+1}, \dots , we can glue the top of the tetrahedron $\Delta_i := \Delta(e_i)$ onto the bottom of Δ_{i+1} in $T \times \mathbb{R}$, because $\tau_+(e_i) = \tau_-(e_{i+1})$. We thus get a bi-infinite stack of tetrahedra $(\Delta_i)_{i \in \mathbb{Z}}$. For any $N > 0$ the space $U_N := \bigcup_{i=-N}^N \Delta_i$ is a strong deformation retraction of $T \times \mathbb{R}$. For N large enough, U_N is homeomorphic to $T \times \mathbb{R}$: the only way this can fail is if all the Δ_i for $-N \leq i \leq N$ have a common edge; but any edge of any tetrahedron Δ_j is shared by only finitely many other (consecutive) Δ_i 's, because for any Farey vertex v , only

finitely many of the Farey edges e_i bound triangles with v as a vertex (and these e_i are consecutive). Therefore, the space $U = \bigcup_{i \in \mathbb{Z}} \Delta_i$ is homeomorphic to $T \times \mathbb{R}$. If m is the period of the word Ω , there is an orientation-preserving homeomorphism Φ of U , acting like $[\varphi]$ on the T -factor, that sends Δ_i to Δ_{i+m} for all i . The quotient U/Φ is a manifold (homeomorphic to) V_φ , naturally triangulated into m ideal tetrahedra.

Figure 2 also shows a way to interpret the standard transvection matrices R and L directly as adjunctions of new tetrahedra (by performing diagonal exchanges on the top faces).

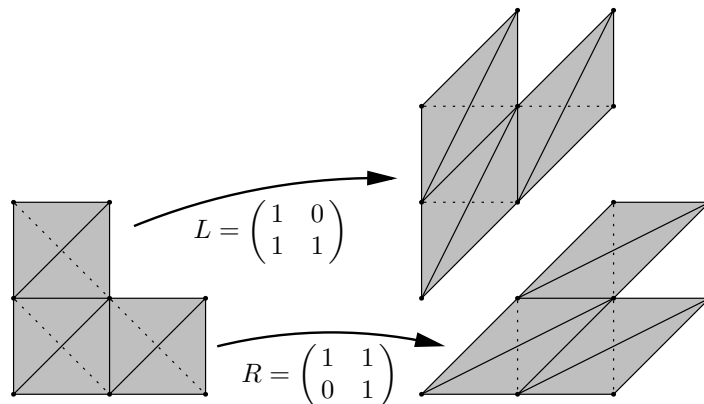


FIGURE 2.

4. COMBINATORICS OF THE TORUS AT INFINITY

The manifold V_φ is naturally homeomorphic to the interior of a compact manifold with boundary, noted $\overline{V_\varphi}$ and defined as a bundle over the circle with fiber $T - \delta$, where δ is a regular neighborhood of the puncture.

The *torus at infinity* of the manifold V_φ is the boundary of $\overline{V_\varphi}$, namely a topological torus. The links of the vertices of the tetrahedra Δ_i provide a tessellation \mathcal{A} of the torus at infinity into topological triangles. In this section we investigate the combinatorics of \mathcal{A} .

Each vertex of \mathcal{A} corresponds to an edge of V_φ shared by a few consecutive tetrahedra Δ_i . This edge in turn corresponds to a Farey vertex shared by a few consecutive Farey triangles. The union of all the Farey triangles adjacent to a given vertex v forms a *fan*. If v arises as a vertex of triangles visited by the line D , one of the following two things must happen right after D enters the fan: either D makes a Right, then a number of Lefts (possibly 0), then a Right and leaves the fan; or the same is true, exchanging Right and Left.

Therefore, the vertices of \mathcal{A} correspond exactly to the subwords of Ω of the form RL^*R or LR^*L (where $*$ ≥ 0). Each such subword actually corresponds to two vertices of \mathcal{A} , because the edges of the tetrahedra Δ_i have two ends.

Moreover, each tetrahedron Δ_i , having four vertices, contributes exactly four triangles to \mathcal{A} . By looking at a vertex (puncture) of the cover $(\mathbb{R}^2 \setminus \mathbb{Z}^2) \times \mathbb{R}$ of $T \times \mathbb{R}$ with embedded Δ_i , one checks (Figure 3) that each of the four triangles has exactly one vertex not shared with any of the other three: we call this vertex

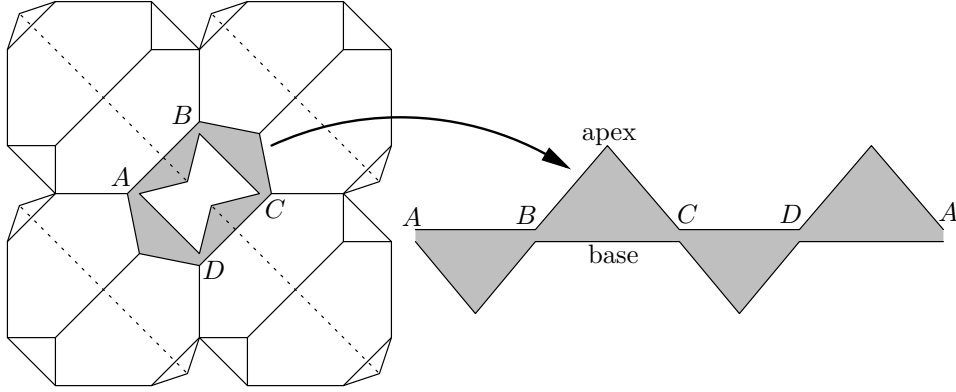


FIGURE 3. The link of the puncture.

the *apex* and the opposite edge the *base*. The four bases form a broken line of four segments which is a closed curve running around the puncture, and the four apices point alternatively up and down in the \mathbb{R} -factor. Such chains of four triangles must be stacked on top of one another while respecting the previously described combinatorics of the vertices. The result is shown in Figure 4, where the underlying word Ω was chosen to be $\dots R^4 L^4 R^4 L^4 \dots$ (read from bottom to top). A few remarks are in order.

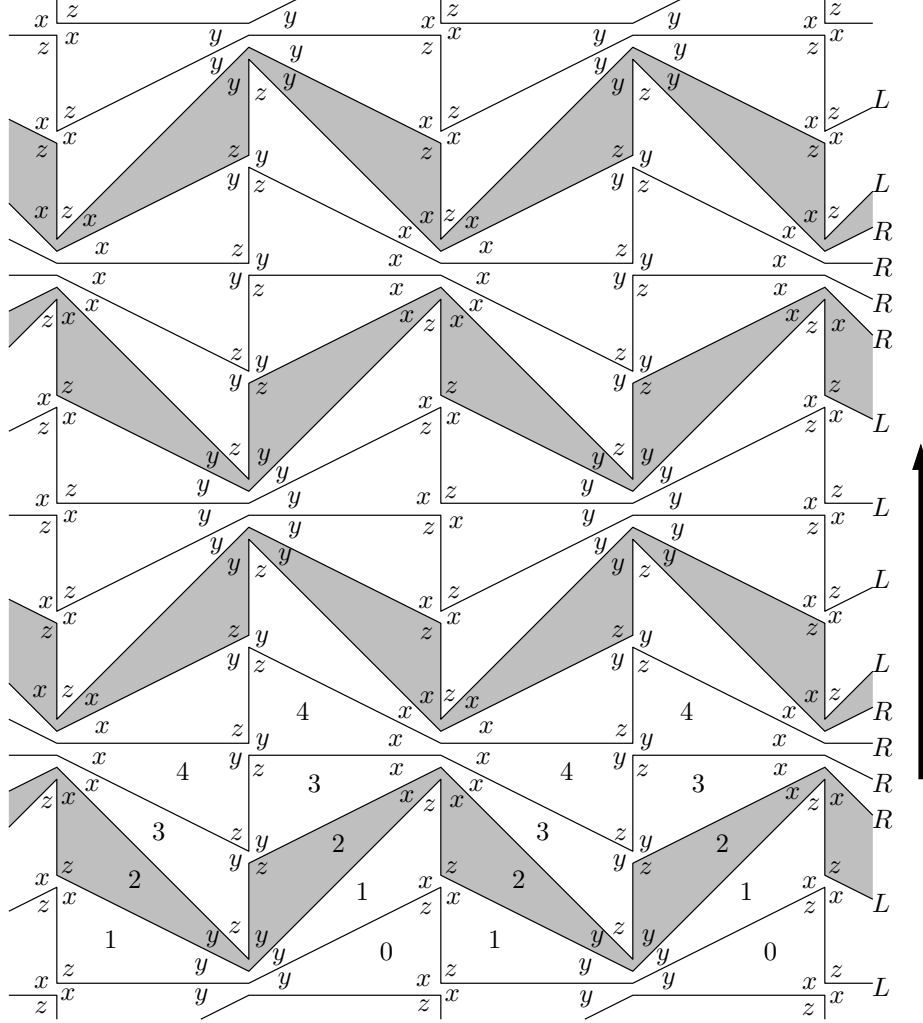
First remark: we labelled by x_i, y_i, z_i the angular sectors of the triangles corresponding to the tetrahedron Δ_i (in Figure 4, the subscript i is replaced by a number at the center of the triangle, omitted after the first few levels). Each angular sector corresponds to a (topological) dihedral angle of Δ_i . Opposite dihedral angles are equal in ideal hyperbolic tetrahedra: this is why three different labels per level are enough (instead of six, the total number of edges in a tetrahedron).

Second remark: the design in Figure 4 of the vertices of the torus at infinity, represented as being “opened up”, is intended to emphasize the layered structure of the picture (each layer corresponds to one tetrahedron Δ_i).

Third remark: the ultimate goal of this paper is to realize Figure 4 geometrically in the plane by Euclidean triangles, making same-layer angles with identical labels equal (Lemma 4 will make this statement more precise).

Fourth remark: the convention is that the pair of edges of Δ_i that does not get identified into one edge is labelled z_i . Equivalently, if a tetrahedron is seen as a diagonal exchange, z_i is the label common to the appearing and disappearing edges. The other edge pairs are labelled in such a way that in each triangle the letters x, y, z appear *clockwise* in that order. Therefore, if e_i is a Farey edge and p (resp. q) its right (resp. left) end for the transverse orientation, the dihedral angle of the tetrahedron Δ_i at the edge of slope p (resp. q) is x_i (resp. y_i).

Fifth remark: the tetrahedra Δ_i are naturally indexed in $\mathbb{Z}/m\mathbb{Z}$. The letters R and L live naturally on the pleated surfaces, or *between* the tetrahedra Δ_i . In Figure 4 and henceforth, the i -th layer is colored in grey iff the letters just before and just after Δ_i are different (here $i = 2, 6, \dots$). Such indices i are called *hinge* indices,

FIGURE 4. The tessellation \mathcal{A} .

because they are at the hinge between two nonempty subwords R^p and L^q . Hinge tetrahedra (the associated Δ_i) will play an important role later on.

Sixth remark: while the fundamental domain of Figure 4 is supposed to have a horizontal length of four triangles (see Figure 3), we notice a horizontal period of length only two. This corresponds to the “hyperelliptic” involution of the punctured torus (rotation of 180° around the puncture, central in $SL_2(\mathbb{Z})$ and therefore well-defined on V_φ). This will simplify some of our computations.

Seventh remark: The valence of a vertex s corresponding to a subword RL^nR or LR^nL of Ω (where $n \geq 0$) is $2n + 4$. This is because exactly $n + 2$ Farey triangles are adjacent to the corresponding rational v_s ; each such Farey triangle defines a triangulated surface (with an edge of slope v_s), and each such surface contributes exactly two segments issued from s in \mathcal{A} .

5. FINDING POSITIVE ANGLES

The tetrahedra Δ_i and Δ_{i+1} have two common triangular faces whose union forms a *pleated punctured torus* Σ homotopic to $T \times \{*\}$ in $T \times \mathbb{R}$. Moreover, Σ receives a transverse orientation from the \mathbb{R} -factor. Suppose all tetrahedra Δ_i are endowed with dihedral angles. Let e be an edge of Σ : if the sum of all dihedral angles at e below Σ is $\pi + \alpha$, we call α the *pleating angle* of Σ at e .

In this section we find positive dihedral angles for the ideal tetrahedra Δ_i . More precisely, we describe the convex space Π of positive angles x_i, y_i, z_i for the Δ_i such that:

$$(1) \quad \begin{cases} \text{i} \text{ ---} & \text{For each } i \text{ in } \mathbb{Z}/m\mathbb{Z} \text{ one has } x_i + y_i + z_i = \pi; \\ \text{ii} \text{ ---} & \text{The dihedral angles around any edge add up to } 2\pi; \\ \text{iii} \text{ ---} & \text{For each } i \text{ in } \mathbb{Z}/m\mathbb{Z}, \text{ the three pleating angles of the pleated} \\ & \text{punctured torus between } \Delta_i \text{ and } \Delta_{i+1} \text{ add up to } 0. \end{cases}$$

Condition (1-ii) is necessary, though not sufficient, for a hyperbolic structure at the edges; Condition (1-iii) is necessary to make the loop around the puncture of T a parabolic isometry of \mathbb{H}^3 .

Recall the line D that runs from the repulsive fixed point q^- to the attractive fixed point q^+ of φ across the Farey triangulation. If the tetrahedron Δ_i , corresponding to the Farey edge e_i , realizes a diagonal exchange that kills an edge ε' and replaces it with ε , we denote by z_i the interior dihedral angle of Δ_i at ε and ε' (fourth remark to Figure 4). Observe that the slope of ε (resp. ε') is the rational located opposite e_i in the Farey diagram, on the side of q^+ (resp. q^-). We define a real number w_i by: $\pi - 2w_i = z_i$.

Thus, if (1-ii) and (1-iii) are to be satisfied, the pleating angles of the pleated punctured torus Σ living between Δ_i and Δ_{i+1} must be

$$(2) \quad -2w_i \text{ , } 2w_{i+1} \text{ and } 2w_i - 2w_{i+1} \text{ .}$$

(Observe the signs: by our definition, angles pointing upwards, like the “new” edge of Δ_i , are negative pleatings, while angles pointing downwards, like the “old” edge of Δ_{i+1} , are positive ones). We write the numbers (2) in the corners of the corresponding Farey triangle (Figure 5 — top), distinguishing the cases L and R , and we repeat this for all indices i .

In fact, the values of the w_i will also determine the x_i and y_i . To see this, we must write down the pleating angles of *two* pleated surfaces, living above *and* below the tetrahedron Δ_i . For notational convenience, write

$$(w_{i-1}, w_i, w_{i+1}) =: (a, b, c).$$

By the fourth remark to Figure 4, the quantity $2x_i$ (resp. $2y_i$) is the difference between the numbers written just above and just below the right (resp. left) end of e_i in Figure 5 (the factor 2 comes from the fact that the two edges of Δ_i with angle x_i [resp. y_i] are identified). By computing differences between the pleating angles given in Figure 5 (bottom), we find the following formulae for x_i, y_i, z_i (depending on the letters Ω_i^- and Ω_i^+ , each equal to R or L , living respectively just before and just after the index i):

$$(3) \quad \begin{array}{c|cc|cc|cc|cc} \Omega_i^-, \Omega_i^+ & L & L & R & R & L & R & R & L \\ \hline x_i & & a+c & -a+2b-c & & a+b-c & & -a+b+c \\ y_i & -a+2b-c & & a+c & & -a+b+c & & a+b-c \\ z_i & & \pi-2b & \pi-2b & & \pi-2b & & \pi-2b \end{array}$$

6. HYPERBOLIC VOLUME

Our goal for the remainder of the paper is to find a point (w_i) of P where the tetrahedra fit together so as to yield a complete hyperbolic structure on V_φ . This section is devoted to checking that this is the same as finding in P a critical point of the total hyperbolic volume, an approach pioneered by Rivin [Ri]. A few facts concerning the volume of ideal tetrahedra will be needed.

6.1. Volume of an ideal tetrahedron. The volume of a hyperbolic tetrahedron whose dihedral angles are $x, y, z > 0$ is

$$(5) \quad \mathcal{V}(x, y, z) = - \int_0^x \log(2 \sin u) du - \int_0^y \log(2 \sin u) du - \int_0^z \log(2 \sin u) du$$

(we refer to [Mi] for a proof). Since $\int_0^\pi \log(2 \sin u) du = 0$, Equation (5) easily implies

Proposition 3. *The function \mathcal{V} can be continuously extended by 0 to all non-negative triples (x, y, z) such that $x + y + z = \pi$. If $\frac{d}{dt}(x_t, y_t, z_t) = (\xi, \eta, \zeta)$ then*

$$(6) \quad \exp\left(\frac{-d}{dt}\mathcal{V}(x_t, y_t, z_t)\right) = \sin^\xi x_t \sin^\eta y_t \sin^\zeta z_t.$$

Proof. Straightforward. We will always apply this formula exactly in the form it is stated, because it will usually make the right hand side simplest. \square

6.2. Critical volume and trivial holonomy.

Lemma 4 (Rivin, Chan–Hodgson). *On the open affine polyhedron P of sequences (w_i) satisfying (4), define the volume functional \mathcal{V} as the sum of the hyperbolic volumes of tetrahedra Δ_i with dihedral angles x_i, y_i, z_i , as given by Table 3. Then (w_i) is a critical point for \mathcal{V} in P if and only if the gluing of the tetrahedra Δ_i defines a complete finite-volume hyperbolic structure on the punctured-torus bundle V_φ .*

Proof. This now standard fact holds for general ideal triangulations as well (see for example [CH, Ri]). The following proof, however, is deliberately specific to the example at hand. This will enable us to introduce a few objects and relationships that will be useful in the sequel.

First we assume (w_i) is critical. Let B be the torus at infinity of V_φ with the vertices of the tessellation \mathcal{A} removed. If σ is the hyperelliptic involution (acting as a translation on B), define $B' = B/\sigma$ and $\mathcal{A}' = \mathcal{A}/\sigma$. Let t_0 be a triangle of \mathcal{A}' , e_0 an oriented edge of t_0 and x_0 an interior point of t_0 . The group of orientation-preserving similarities of the Euclidean plane \mathbb{C} is $\mathbb{C}^* \ltimes \mathbb{C}$.

Definition 5. For a given (w_i) in P , the *holonomy function* is the representation

$$\rho : \pi_1(B', x_0) \rightarrow \mathbb{C}^* \ltimes \mathbb{C}$$

defined as follows. Given an element α of $\pi_1(B', x_0)$, view α as a cyclic sequence of triangles $t_0, t_1, \dots, t_s = t_0$ of \mathcal{A}' , such that any two consecutive t_i 's share an edge. Then, draw an oriented copy τ_0 of t_0 in the plane \mathbb{C} , with angles specified by (w_i) , by making the image of the oriented edge e_0 coincide with $(0, 1)$. Sharing an edge with τ_0 , draw a copy τ_1 of t_1 , also with angles specified by (w_i) . Then draw a copy τ_2 of t_2 adjacent to τ_1 , etc. By definition, $\rho(\alpha)$ is the orientation-preserving

similarity mapping the copy of the oriented edge e_0 in τ_0 to the copy of e_0 in τ_s . The *reduced holonomy function* $\psi : \pi_1(B', x_0) \rightarrow \mathbb{C}^*$ is defined as the projection of ρ on the first factor.

It is a simple exercise to check that ρ is well-defined, and is a representation (the concatenation rule being that $\alpha\beta$ denotes the path α followed by the path β). Note that ψ , having a commutative target, factors through a representation $\psi : H_1(B', \mathbb{Z}) \rightarrow \mathbb{C}^*$.

Sublemma 6. *Let α be an element of $H_1(B', \mathbb{Z})$ represented by a curve around a 4-valent vertex of \mathcal{A}' , and let β be represented by a curve that follows a “grey” (hinge) level in \mathcal{A}' (Figure 7). If (w_i) is critical for the volume functional \mathcal{V} , then $\psi(\alpha) = \psi(\beta) = 1$.*

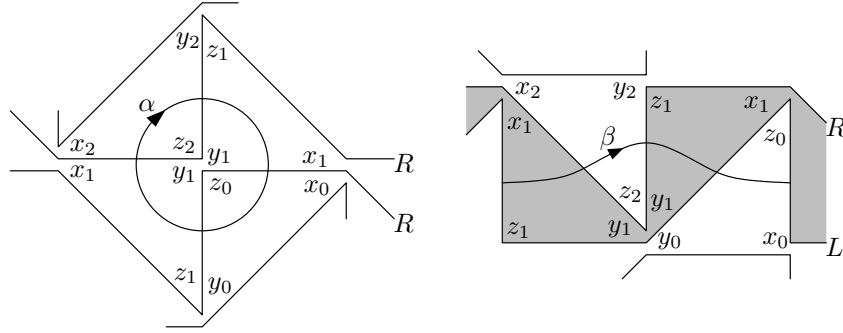


FIGURE 7.

Proof. We already know that $\psi(\alpha), \psi(\beta)$ belong to \mathbb{R}_+^* , because the angle conditions (1) defining P impose oriented parallelism. It remains to prove that $|\psi(\alpha)| = |\psi(\beta)| = 1$.

At a critical point, the partial derivatives of \mathcal{V} with respect to any of the w_i must vanish. Between and near two identical letters, say R and R , according to Table (3), the angles are

Ω		R	R
i		0	1
w_i		a	b
x_i	$\xi - b$	$-a + 2b - c$	$-b + \xi'$
y_i	$\eta + b$	$a + c$	$b + \eta'$
z_i	$\pi - 2a$	$\pi - 2b$	$\pi - 2c$

(the exact expression of ξ, ξ', η, η' depends on the letters before and after RR , but only the b -contribution matters here). Using Proposition 3, criticality of \mathcal{V} implies

$$1 = \exp \frac{-\partial \mathcal{V}}{\partial b} = \frac{\sin y_0 \sin^2 x_1 \sin y_2}{\sin x_0 \sin^2 z_1 \sin x_2}.$$

Using the fact that edge lengths in a triangle are proportional to angle sines, it follows that the edge lengths in Figure 7 (left) around the central vertex fit nicely together. So $|\psi(\alpha)| = 1$. The case of a subword LL is treated similarly, which takes care of *all* 4-valent vertices of the tessellation \mathcal{A}' .

Near a hinge between two different letters, say L followed by R , the angles are

Ω	L	R
i	0	1
w_i	a	b
x_i	$\xi + b$	$a + b - c$
y_i	$\eta - b$	$-a + b + c$
z_i	$\pi - 2a$	$\pi - 2b$

This time, criticality implies

$$1 = \exp \frac{-\partial \mathcal{V}}{\partial b} = \frac{\sin x_0 \sin y_1 \sin x_1 \sin y_2}{\sin y_0 \sin^2 z_1 \sin x_2}.$$

As shown in Figure 7 (right) and by the same trigonometric argument, this means that the first and last edges crossed by β have the same length. So $\psi(\beta) = 1$. (If Ω is reduced to LR , the computation is formally the same, identifying indices 0 and 2). The case of a subword RL is similar. Sublemma 6 is proved. \square

Now let α be an element of $\pi_1(B', x_0)$ that is conjugated to a simple loop around a 4-valent vertex of \mathcal{A}' . By Sublemma 6 (and an easy conjugation argument), $\rho(\alpha)$ is a translation. Moreover, $\rho(\alpha)$ fixes the vertex around which α revolves, so $\rho(\alpha) = 1$, the identity of the Euclidean plane.

Sublemma 7. *Let U be the quotient of the torus at infinity of V_φ by the hyperelliptic involution, so that $B' \subset U$. Suppose (w_i) is critical for \mathcal{V} . Then the representation $\rho : \pi_1(B', x_0) \rightarrow \mathbb{C}^* \ltimes \mathbb{C}$ descends to a representation $\rho_U : \pi_1(U, x_0) \rightarrow \mathbb{C}^* \ltimes \mathbb{C}$ whose first projection $\psi_U : \pi_1(U, x_0) \rightarrow \mathbb{C}^*$ is trivial.*

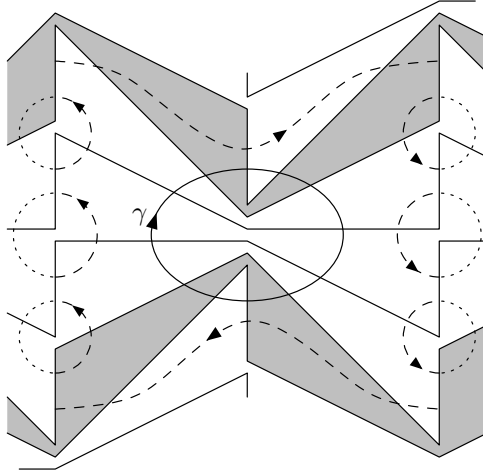


FIGURE 8.

Proof. To see that ρ_U is well-defined, we only need to check that, if γ is (conjugated to) a loop around a vertex v of \mathcal{A}' , then $\rho(\gamma) = 1$. If v has valence 4, it has already been done. If not, by the argument preceding Sublemma 7, it is sufficient to check that $\psi([\gamma]) = 1$, where $[\gamma]$ denotes the homology class of γ . But in $H_1(B', \mathbb{Z})$, the element $[\gamma]$ is a sum of loops around 4-valent vertices and curves following “grey”

levels (see Figure 8: the vertical edges of B' on the two sides of the picture are identified, and the curves crossing these edges undergo a “split-and-paste” process to yield γ). So by Sublemma 6, $\psi([\gamma]) = 1$: therefore ρ_U is well-defined. Moreover, if β is a curve following a “grey” level, Sublemma 6 tells that $\rho_U(\beta) = \rho(\beta)$ is a non-identical Euclidean *translation*. The value of ρ_U on another generator of $\pi_1(U)$ (which is abelian) must commute with $\rho_U(\beta)$, and therefore be a translation too. So ρ_U has its image contained in $\{1\} \times \mathbb{C}$ and $\psi_U = 1$: Sublemma 7 is proved. \square

By assigning length 1, for example, to the reference edge e_0 of \mathcal{A}' , a critical point (w_i) of the volume functional thus defines the lengths of all other edges of \mathcal{A}' in a coherent way. This yields a complete Euclidean metric g on U . The universal cover \tilde{U} of U thus embeds into \mathbb{C} (the embedding, also called the developing map of the local Euclidean structure, can only be injective, because the \tilde{g} -geodesic joining two distinct points of \tilde{U} is sent to a geodesic of \mathbb{C}); so there is an isometry $\tilde{U} \simeq \mathbb{C}$. The metric g lifts from U to the torus at infinity of V_φ and its tessellation \mathcal{A} , producing a geometric realization of \mathcal{A} and Figure 4 in \mathbb{C} (Euclidean plane tiling). Above each triangle of the universal cover of \mathcal{A} now sits one ideal tetrahedron with vertex at infinity: the tetrahedron is the hyperbolic convex hull of ∞ and the vertices of the triangle. Note that these tetrahedra fill \mathbb{H}^3 completely above a certain height.

To make sure that the pasted metric on the union $V = V_\varphi$ of all ideal tetrahedra must then be complete, assume a geodesic $\gamma(t)$ in V hits infinity at time $T < \infty$. If $K \subset V$ is compact, i.e. has a compact intersection with each tetrahedron Δ_i , then γ must eventually exit K (if not, the $\gamma(T - 1/n)$ accumulate at some point p of some tetrahedron, but centered at p there is a small embedded hyperbolic ball: absurd). So for t sufficiently close to T , there is a lift of $\gamma(t)$ arbitrarily high above the tessellation \mathcal{A} (embedded in \mathbb{C} in the upper half space model). But at sufficiently great height, the tetrahedra above \mathcal{A} fill \mathbb{H}^3 completely, so geodesics are defined for long times (e.g. times larger than 1): a contradiction. The first implication of Lemma 4 is proved.

To prove the converse, it is enough to show that if the gluing of the tetrahedra yields a complete hyperbolic metric, then the gluing of their vertex links yields a geometric realization of \mathcal{A} , i.e. of Figure 4 (checking $\partial\mathcal{V}/\partial w_i = 0$ then amounts to a rerun of the two computations in Sublemma 6, distinguishing whether i is a hinge index or not). But the latter is clear: given a complete hyperbolic metric, consider a triangulated universal cover $\mathbb{H}^3 \rightarrow V_\varphi$ and send (a lift of) the cusp to infinity in the upper half space model. It is a classic argument that deck transformations of \mathbb{H}^3 which fix infinity must be parabolic, so the link of infinity has two translational periods and provides a Euclidean realization of \mathcal{A} (and of Figure 4). \square

6.3. Behavior of the volume functional. As a consequence of Lemma 4, to prove Theorem 1 we only need to find a critical point of the volume functional \mathcal{V} in the open polyhedron P of cyclic sequences (w_i) satisfying the conditions (4). A few more facts about the volume of ideal hyperbolic tetrahedra will be needed.

By Proposition 3, the volume functional \mathcal{V} continuously extends to the (compact) closure \overline{P} of the polyhedron P (the space \overline{P} is defined by turning the conditions (4) to weak inequalities, or taking the limits in \mathbb{R}^m of sequences of P). Then \mathcal{V} has well-defined extrema on \overline{P} , which are automatically critical if they belong to

P . Because of the following proposition, the only possibility for a critical point is to be an absolute maximum.

Proposition 8. *The volume of an ideal tetrahedron is a concave function of its dihedral angles.*

Proof. This follows from Proposition 3, whose notations we use again: x_t, y_t, z_t are the dihedral angles. By symmetry we may assume $x_0, y_0 \leq \pi/2$. Assume further that x_t, y_t, z_t are affine functions of t with first-degree coefficients ξ, η, ζ . Proposition 3 implies $-d\mathcal{V}/dt = \xi \log \sin x_t + \eta \log \sin y_t + \zeta \log \sin z_t$, and by differentiating:

$$\begin{aligned} -d^2\mathcal{V}/dt^2|_{t=0} &= \xi^2 \cot x_0 + \eta^2 \cot y_0 + \zeta^2 \cot z_0 \\ &= \xi^2 \cot x_0 + \eta^2 \cot y_0 + (\xi + \eta)^2 \frac{1 - \cot x_0 \cot y_0}{\cot x_0 + \cot y_0} \\ &= \frac{(\xi + \eta)^2 + (\xi \cot x_0 - \eta \cot y_0)^2}{\cot x_0 + \cot y_0} \geq 0. \end{aligned}$$

□

As a consequence, the volume functional \mathcal{V} is also concave on \overline{P} and Theorem 1 holds if the maximum of \mathcal{V} is interior. Next we explore the behavior of \mathcal{V} near the boundary of \overline{P} .

Proposition 9. (Simple degeneracy). *If $(Q_t)_{t \geq 0}$ is a smooth family of ideal tetrahedra with dihedral angles x_t, y_t, z_t such that $x_0, y_0 \in (0, \pi)$; $z_0 = 0$ and $\frac{dz_t}{dt}|_{t=0} > 0$, then $\frac{d\mathcal{V}}{dt}|_{t=0} = +\infty$.*

Proof. Simply check that the right hand side of (6) goes to 0 as t goes to 0. We call this situation *simple degeneracy* because the limiting triangle has only one vanishing angle (two of its vertices are therefore collapsed). □

Proposition 10. (Double degeneracy). *If $(Q_t)_{t \geq 0}$ is a smooth family of ideal tetrahedra satisfying $(x_0, y_0, z_0) = (0, 0, \pi)$ and $\frac{d}{dt}|_{t=0}(x_t, y_t, z_t) = (1 + \lambda, 1 - \lambda, -2)$ with $\lambda \in (-1, 1)$, then $\exp \frac{-d\mathcal{V}}{dt}|_{t=0} = \frac{1-\lambda^2}{4} \left(\frac{1+\lambda}{1-\lambda} \right)^\lambda$.*

Proof. As t goes to 0, one has $\sin x_t \sim (1 + \lambda)t$ and $\sin y_t \sim (1 - \lambda)t$ and $\sin z_t \sim 2t$. The right hand side of (6) is thus equivalent to

$$[(1 + \lambda)t]^{1+\lambda}[(1 - \lambda)t]^{1-\lambda}(2t)^{-2} = \frac{1 - \lambda^2}{4} \left(\frac{1 + \lambda}{1 - \lambda} \right)^\lambda.$$

We call this situation *double degeneracy* because the limiting triangle has two vanishing angles (its vertices are distinct, but collinear). □

7. RULING OUT SOME DEGENERACIES

From now on, we fix (w_i) in the compact polyhedron \overline{P} at a point which maximizes the total hyperbolic volume of all tetrahedra. To prove that (w_i) is critical for the volume \mathcal{V} , we only need to make sure that (w_i) lies in the interior P of \overline{P} , i.e. that all x_i, y_i, z_i lie in $(0, \pi)$.

Proposition 11. *If for some index i , one of the numbers x_i, y_i, z_i is 0, then two of them are 0 and the third is π . In other words, there are no simple degeneracies, only double degeneracies.*

Proof. If not, consider an affine segment from (w_i) to some interior point of P . By Proposition 9, the partial derivative of \mathcal{V} at (w_i) along that segment is infinite positive, so \mathcal{V} was not maximal at (w_i) . \square

Tetrahedra Δ_i such that (x_i, y_i, z_i) has one, and therefore two vanishing terms are called *flat*, and are characterized by the property that w_i is either 0 or $\frac{\pi}{2}$.

Proposition 12. (Domino effect). *If two consecutive tetrahedra Δ_{i-1}, Δ_i are flat, then Δ_{i+1} is flat, too.*

Proof. We use only Table (3). There are several cases:

- If i is not a hinge index, flatness of Δ_i implies $w_{i-1} + w_{i+1} \in \{0, \pi\}$. By the range condition $0 \leq w \leq \frac{\pi}{2}$, this implies $w_{i+1} \in \{0, \frac{\pi}{2}\}$, so Δ_{i+1} is flat.
- If i is a hinge index and $w_i = \frac{\pi}{2}$, we must have $|w_{i-1} - w_{i+1}| = \frac{\pi}{2}$, so by the range condition, w_{i+1} is 0 or $\frac{\pi}{2}$, and Δ_{i+1} is flat.
- If i is a hinge index and $w_i = 0$, we must have $|w_{i+1} - w_{i-1}| \leq 0$ so $w_{i+1} = w_{i-1}$: but Δ_{i-1} is assumed flat, and therefore, so is Δ_{i+1} . Note that flatness of Δ_{i-1} was needed only in this case. \square

Proposition 13. *If Δ_i is flat, then i is a hinge index and $w_i = 0$.*

Proof. In all other cases, the proof of Proposition 12 actually forces Δ_{i+1} to be flat, which triggers a domino effect: all Δ_j 's are flat, and the volume is 0 — certainly not maximal. \square

Easy Fact 14. If ABC is a Euclidean triangle with positive angles and edge lengths a, b, c , then

$$\begin{aligned} a = b &\iff \hat{A} = \hat{B} \iff \sin \hat{A} = \sin \hat{B} \\ a < b &\iff \hat{A} < \hat{B} \iff \sin \hat{A} < \sin \hat{B}. \quad \square \end{aligned}$$

The volume \mathcal{V} is still supposed maximal, and we assume that some tetrahedra Δ_i are flat, i.e. that some hinge parameters w_i vanish. Places where a parameter w_i vanishes will be signalled by a vertical bar: $\dots LL|RR\dots$. By Proposition 12, consecutive vertical bars are always separated by at least two letters.

The patterns $RL|RL$ and $LR|LR$ can never occur, because increasing the incriminated w_i to ε would automatically increase the volume (note that $w_{i-1} = w_{i+1} =: A$ by the hinge condition 4-iii):

Ω	L	R	L	R
w_i	u	A	$0 + \varepsilon$	A
x_i	.	$u + A - \varepsilon$	ε	$\varepsilon + A - v$
y_i	.	$-u + A + \varepsilon$	ε	$-\varepsilon + A + v$
z_i	.	$\pi - 2A$	$\pi - 2\varepsilon$	$\pi - 2A$

$$\exp \frac{-\partial \mathcal{V}}{\partial \varepsilon} \Big|_{\varepsilon=0} = \frac{1}{4} \cdot \frac{\sin(A-u) \sin(A-v)}{\sin(A+u) \sin(A+v)} < 1$$

where we used the Easy Fact 14, Proposition 3 and Proposition 10 (with $\lambda = 0$).

Any vertical bar thus lives next to at least two consecutive identical letters (on at least one side). However, the patterns $R|LL|R$ and $L|RR|L$ are also prohibited by Proposition 13, since the central (non-hinge) tetrahedron would have one vanishing angle ($a + c = 0$ in the notations of Table 3).

8. A GEOMETRICAL LEMMA

Definition 15. In the universal cover of the tessellation \mathcal{A} of the torus at infinity of V_φ (Figure 4), a *fan* is a sequence of at least three consecutive layers, such that the first and last layers are grey and all layers inbetween are white. Fans are in bijection with the subwords of Ω of the form RL^kR or LR^kL with $k \geq 2$ (see the remarks to Figure 4 in Section 4).

Lemma 16. *Suppose $w_0 = 0$, so that Ω contains a subword $L|R^kL$ with $k \geq 2$, or $L|R^k|L$ with $k \geq 3$ (in the latter case, the second bar indicates that w_k vanishes as well as w_0). The corresponding fan admits a complete Euclidean structure with boundary (with angles prescribed by the w_i 's). Moreover, let Q, P, T be the lengths of the segments of the broken line corresponding to the first R , in the order indicated in Figure 9 (P, T are the sides adjacent to the apex in a flat upward-pointing grey [hinge] triangle, in the sense of Figure 3 page 6). Then $Q < P + T$.*

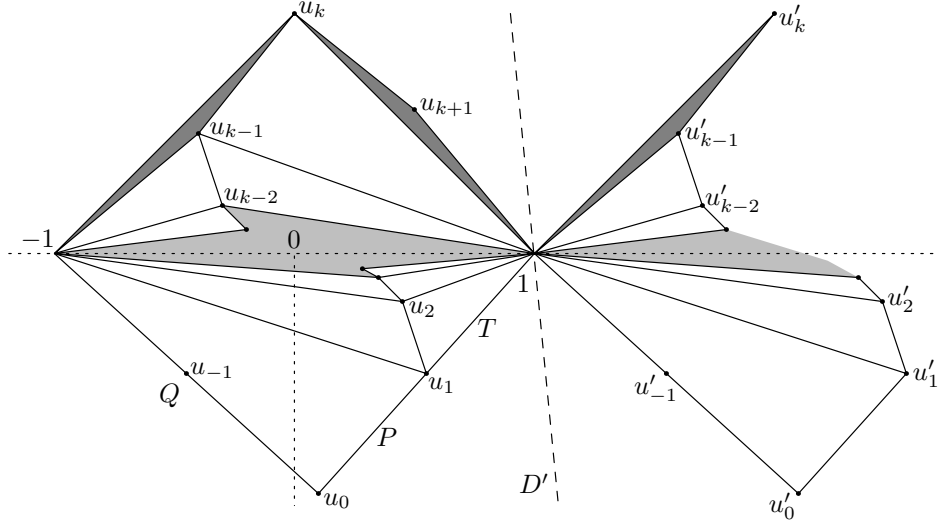


FIGURE 9. This situation, where $Q \geq P + T$, cannot hold.

Proof. We first restrict our attention to the case $L|R^kL$, $k \geq 2$. The interior vertices of the topological fan correspond to the indices i living between two R 's, i.e. $1 \leq i \leq k-1$, in the sense that holonomy around the i -th vertex u_i (Figure 9) is controlled by $\partial\mathcal{V}/\partial w_i$ (Sublemma 6). When $2 \leq i \leq k-1$, none of the triangles adjacent to u_i are flat, so w_i can vary in a small interval without making the m -tuple w exit the domain \bar{P} ; consequently, the value of w_i in that interval is critical, which by the computation of Sublemma 6 implies that the holonomy around the associated vertex u_i is trivial. As for $i = 1$, the corresponding vertex u_1 is adjacent to a flat angle $z_0 = \pi$ (Figure 9) so its holonomy is not imposed by the w_i 's (when a triangle has an angle π , the other two angles are always 0 while the adjacent sides may have arbitrary lengths). The case of $L|R^k|L$ is similar: for indices $2 \leq i \leq k-2$ Sublemma 6 applies, while for $i = 1$ or $k-1$ holonomy is not imposed by the w_i 's.

Therefore we can embed the fan as an infinite string of triangulated polygons into \mathbb{C} . We make two consecutive nodes (i.e. lifts of the $(2k+4)$ -valent vertex of \mathcal{A} associated to the full subword LR^kL) coincide with -1 and 1 , and also denote by u_i the complex coordinate of the copy of u_i between these nodes (the index i actually ranges from -1 to $k+1$, see Figure 9). We arrange so that $\text{Im}(u_0) < 0$ and u_1 lies on the open segment $(u_0, 1)$. While removing any node disconnects the fan, Condition (1-iii) implies that the image of the embedding is invariant under a horizontal translation of length 2. In particular, the geometric link of each node, such as 1 or -1 , is completely determined. To prove the assertion of the Lemma, it is sufficient to show that $\text{Re}(u_0) < 0$. So assume $\text{Re}(u_0) \geq 0$.

The similarity property of the triangles with vertices $1, u_i, u_{i+1}$ and $-1, u_i, u_{i-1}$ is expressed by the relation $\frac{u_{i+1}-1}{u_i-1} = \frac{u_{i-1}+1}{u_i+1}$, hence by induction

$$(u_{i+1}-1)(u_i+1) = (u_i-1)(u_{i-1}+1) = \cdots = (u_1-1)(u_0+1) =: K.$$

Then, as u_1 sits between 1 and u_0 , the number u_1-1 is a positive (real) multiple of u_0-1 , so K is a positive multiple of u_0^2-1 which implies $\text{Im}(K) \leq 0$. Let D be the line through 0 and the points $\pm\sqrt{K}$: either D is vertical, or D visits the upper-left and lower-right (open) quadrants. Let D' be the line through 1 , parallel to D ; and define $u'_i := 2+u_i$ for all i . By definition of K , the rays $[1, u_{i+1})$ and $[1, u'_i)$ are symmetric with respect to D' . Moreover, the rays through $u_0, u_1, \dots, u_k, u_{k+1}, u'_k, u'_{k-1}, \dots, u'_0, u'_{-1}, u_0$ issued from 1 (in that cyclic order) divide \mathbb{C} into angular sectors of sum 2π realizing the geometric link of a node of the fan, as specified by the angles $x_i, y_i, z_i \geq 0$. Finally, since all these angles are non-negative, the symmetry of the link with respect to D' implies that for all $-1 \leq i \leq k$, the point u'_i (resp. u_{i+1}) is on the right (resp. left) of D' .

Recall $\text{Im}(u_0) < 0$. Suppose $\text{Im}(u_i) < 0$ for some $0 \leq i \leq k$. Then $\text{Im}(u'_i) < 0$. Considering the direction of D' and the symmetry property with respect to D' , this implies $\text{Im}(u_{i+1}) < 0$. By an immediate induction, the angular sector $\widehat{u_{k+1}1u'_k}$ (just above 1) is larger than π . But it is an angle of the link at the node 1 (namely, z_{k+1}). Absurd. \square

Of course, a statement similar to Lemma 16 holds for subwords $LR^k|L$, and also for $R|L^kR$, $R|L^k|R$, $RL^k|R$.

9. RULING OUT ALL DEGENERACIES

Easy Fact 17. If U and V are positive constants, the function defined on $(-1, 1)$ by $f(\lambda) := \frac{1-\lambda^2}{4}U(\frac{1+\lambda}{1-\lambda}V)^\lambda$ takes somewhere the value $\frac{U}{(1+V)(1+V^{-1})}$. It is in fact an absolute minimum: indeed, $(\log f)'(\lambda) = \log[\frac{1+\lambda}{1-\lambda}V]$, so f is minimal when the bracket is 1, hence the result by a direct computation. \square

Now we can prove that the configuration $\dots RR|L\dots$ (and similarly $\dots LL|R\dots$) never occurs, which will imply Theorem 1. The strategy is to suppose $RR|L$, i.e. $w_j = 0$ for some j (for notational convenience we assume $j = 2$). Next, replace w_2 by ε and w_1 by $w_1 + \lambda\varepsilon$, for a wisely chosen λ . The volume \mathcal{V} will then increase. (The value of λ , which does not need to be explicitly computed, will maximize $\partial\mathcal{V}/\partial\varepsilon$, and $e^{-\partial\mathcal{V}/\partial\varepsilon}$ will be the value of f given in Easy Fact 17. We will specify in due time what the parameters U, V are.) Volume computations follow from Proposition 10 (at the index $i = 2$) and Proposition 3 (other indices).

9.1. **Case 1: $RR|LR$.** According to Table (3), the angles are as follows. Note the relation $w_1 = w_3 =: A$, a consequence of the hinge condition (4-iii).

Ω	R		R	$ $	L	R
i	0	1	2		3	4
w_i	u	$A + \lambda\varepsilon$	$0 + \varepsilon$		A	v
x_i	$\xi - A - \lambda\varepsilon$	$-u + 2A + 2\lambda\varepsilon - \varepsilon$	$(1 - \lambda)\varepsilon$		$\varepsilon + A - v$.
y_i	$\eta + A + \lambda\varepsilon$	$u + \varepsilon$	$(1 + \lambda)\varepsilon$		$-\varepsilon + A + v$.
z_i	$\pi - 2u$	$\pi - 2A - 2\lambda\varepsilon$	$\pi - 2\varepsilon$		$\pi - 2A$.

We cannot have $|RR|LR$, so $u > 0$ and Δ_0 is not flat. Therefore, if $-1 < \lambda < 1$, then ε can take small positive values without making any of the x_i, y_i, z_i negative. Compute

$$\begin{aligned} \exp \frac{-\partial \mathcal{V}}{\partial \varepsilon} \Big|_{\varepsilon=0} &= \frac{1 - \lambda^2}{4} \underbrace{\frac{\sin(A - v)}{\sin(A + v)}}_{\leq 1} \underbrace{\frac{\sin y_1}{\sin x_1}}_{Q/P} \left(\frac{1 + \lambda}{1 - \lambda} \underbrace{\frac{\sin y_0 \sin^2 x_1}{\sin x_0 \sin^2 z_1}}_{P/T=:V} \right)^\lambda \\ &\leq \frac{Q/P}{(1 + P/T)(1 + T/P)} = \frac{1}{1 + P/T} \frac{Q}{P + T} < 1 \end{aligned}$$

by Lemma 16 (see Figure 10, left — again, the sine relation in triangles was used to compute Q/P and P/T). If Ω is reduced to $RR|L$, columns 0 and 3 of the table above coincide, but the perturbative terms in ε are added together and the computations are the same.

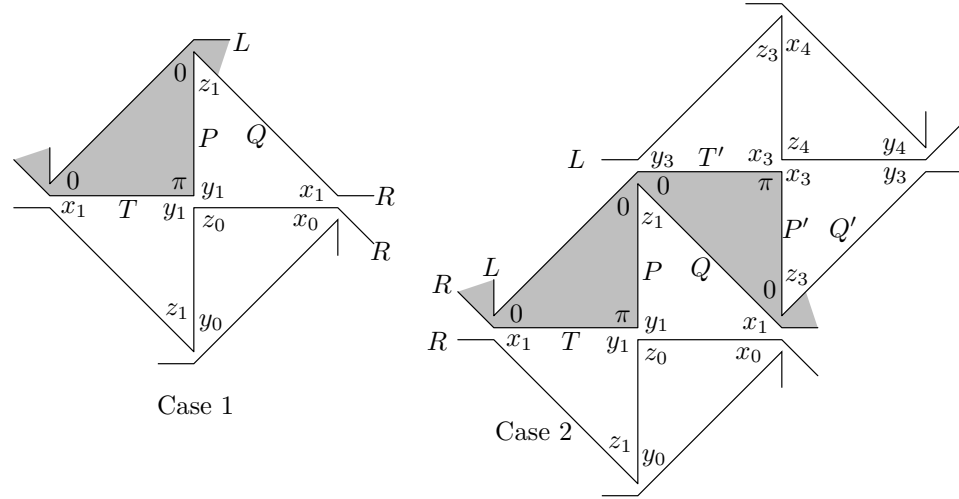


FIGURE 10.

9.2. Case 2: $RR|LL$.

Ω	R		R	L	L	
i	0	1	2	3	4	
w_i	u	$A + \lambda\varepsilon$	$0 + \varepsilon$	A	v	
x_i	$\xi - A - \lambda\varepsilon$	$-u + 2A + 2\lambda\varepsilon - \varepsilon$	$(1 - \lambda)\varepsilon$	$\varepsilon + v$	$A + \xi'$	
y_i	$\eta + A + \lambda\varepsilon$	$u + \varepsilon$	$(1 + \lambda)\varepsilon$	$-\varepsilon + 2A - v$	$-A + \eta'$	
z_i	$\pi - 2u$	$\pi - 2A - 2\lambda\varepsilon$	$\pi - 2\varepsilon$	$\pi - 2A$	$\pi - 2v$	

First consider the value of A . Since there can be no vertical bars immediately before or after $RR|LL$, the tetrahedra $\Delta_0, \Delta_1, \Delta_3, \Delta_4$ have positive angles, so the parameter A (which does not contribute to the angles of any other tetrahedra) can vary freely in an open interval when $\varepsilon = 0$. So A must be critical:

$$1 = \exp \frac{-\partial \mathcal{V}}{\partial A} \Big|_{\varepsilon=0} = \underbrace{\frac{\sin y_0 \sin^2 x_1}{\sin x_0 \sin^2 z_1}}_{P/T} \underbrace{\frac{\sin^2 y_3 \sin x_4}{\sin^2 z_3 \sin y_4}}_{P'/T'}$$

hence $P/T = T'/P'$. Therefore, with the right choice of λ ,

$$\begin{aligned} \exp \frac{-\partial \mathcal{V}}{\partial \varepsilon} \Big|_{\varepsilon=0} &= \frac{1 - \lambda^2}{4} \frac{\overbrace{\sin y_1 \sin x_3}^U}{\underbrace{\sin x_1 \sin y_3}_{Q/P} \underbrace{\sin y_3 \sin x_1}_{Q'/P'}} \left(\frac{1 + \lambda}{1 - \lambda} \frac{\sin y_0 \sin^2 x_1}{\underbrace{\sin x_0 \sin^2 z_1}_{P/T=T'/P'=V}} \right)^\lambda \\ &= \frac{Q/P \cdot Q'/P'}{(1 + T/P)(1 + T'/P')} = \frac{Q}{P + T} \frac{Q'}{P' + T'} < 1 \end{aligned}$$

by Lemma 16 (see Figure 10, right). If Ω is reduced to $RR|LL$, columns 0 and 4 in the table above coincide, but the perturbative terms are added together and the computations are the same. Theorem 1 is proved.

10. A NUMERICAL EXAMPLE: $R^N L^M$

In this section we fix two large enough integers N and M and investigate the behavior of the angles for $\Omega = R^N L^M$: the angles made positive by the previous computations will turn out to be very small. We will directly construct a Euclidean realization of Figure 4, automatically unique up to isometry. Since N and M are large, there exist small complex numbers a, a', b, b' such that

$$(7) \quad \begin{cases} \sin a &= i \tan b \cos b' \\ \sin a' &= -i \tan b' \cos b \end{cases} \quad \text{where} \quad \begin{cases} b &= (\pi - 2a)/N \\ b' &= (\pi - 2a')/M \end{cases}.$$

A way to compute a, a' is to set $a_0 = a'_0 = 0$ and to define inductively $a_{s+1} = \arcsin(i \tan \frac{\pi - 2a_s}{N} \cos \frac{\pi - 2a'_s}{M})$ and a similar expression for a'_{s+1} . The sequences a_s, a'_s converge exponentially fast to a, a' . The constants a, a' become arbitrarily small for large enough N, M , hence $b \sim \pi/N$, $b' \sim \pi/M$ and, plugging into (7), $a \sim i\pi/N$, $a' \sim -i\pi/M$. Using the Landau symbol $O(A, B)$ in the sense of $O(\max\{A, B\})$, this in turn yields

$$(8) \quad \begin{aligned} b &= \frac{\pi}{N} - \frac{2i\pi}{N^2} + O\left(\frac{1}{N^3}, \frac{1}{M^3}\right) & a &= \frac{i\pi}{N} + \frac{2\pi}{N^2} + O\left(\frac{1}{N^3}, \frac{1}{M^3}\right) \\ b' &= \frac{\pi}{M} + \frac{2i\pi}{M^2} + O\left(\frac{1}{N^3}, \frac{1}{M^3}\right) & a' &= \frac{-i\pi}{M} + \frac{2\pi}{M^2} + O\left(\frac{1}{N^3}, \frac{1}{M^3}\right). \end{aligned}$$

Proposition 18. *The fan corresponding to R^N can be embedded into \mathbb{C} with nodes at complex coordinates $\pm \cot b$ and intermediary vertices $\cot(a + sb)$ where $-1 \leq s \leq N + 1$; similarly, the fan corresponding to L^M can be embedded into \mathbb{C} with nodes $\pm \cot b'$ and intermediary vertices $\cot(a' + sb')$ where $-1 \leq s \leq M + 1$ (see Figure 11).*

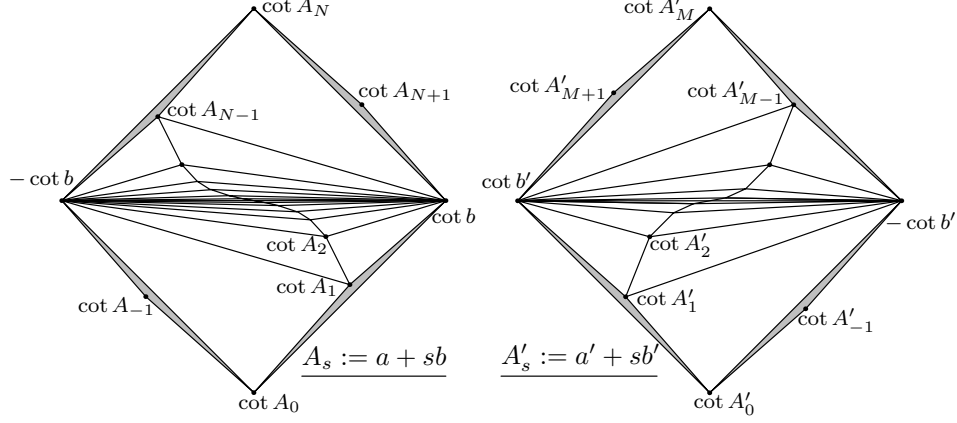


FIGURE 11.

Proof. There are several things to check. First, the congruence of pairs of triangles inside each fan follows from the identity of complex ratios

$$(9) \quad \frac{\cot(A+b) - \cot b}{\cot(A+b) - \cot A} = \frac{\cot(A-b) + \cot b}{\cot(A-b) - \cot A} = \frac{\sin^2 A}{\sin^2 b}$$

where $A = a + sb$ for $0 \leq s \leq N$, and an identical relation for a', b' .

Next, each fan, when stripped of two of its four limiting (grey) triangles, is a parallelogram. This follows from $\cot(a + Nb) = \cot(\pi - a) = -\cot a$, and the same for a' . In particular, each fan admits a center of symmetry.

Furthermore, these two parallelograms are congruent. To see this, denote by $\alpha, \alpha', \beta, \beta'$ the squared cotangents of a, a', b, b' . Raising (7) to the power -2 , we get

$$\begin{cases} 1 + \alpha &= -\beta(1 + \beta'^{-1}) \\ 1 + \alpha' &= -\beta'(1 + \beta^{-1}) \end{cases} \quad \text{hence} \quad \frac{\alpha}{\alpha'} = \frac{\beta + \beta/\beta' + 1}{\beta' + \beta'/\beta + 1} = \frac{\beta}{\beta'}$$

which implies $\frac{\cot a}{\cot b} = \pm \frac{\cot a'}{\cot b'}$, the correct sign being minus by the estimates (8).

Further yet, the limiting (grey) triangles of the two fans have the same shape: by (9) their complex ratios are $\frac{\sin^2 a}{\sin^2 b}$ and $\frac{\sin^2 b'}{\sin^2 a'}$, both equal by (7) to $-\frac{\cos^2 b'}{\cos^2 b}$.

Finally, all triangles are positively oriented, i.e. $\text{Im}(\frac{\sin^2 A_s}{\sin^2 b}) > 0$ for $A_s = a + sb$ and $0 \leq s \leq N$. We first check this for $s = 0$ (the case $s = N$ will follow by symmetry): we have $\frac{\sin^2 a}{\sin^2 b} = -\frac{\cos^2 b'}{\cos^2 b} = -\frac{1 - \sin^2 b'}{1 - \sin^2 b}$. In the latter expression, both the numerator and denominator are ~ 1 , but their imaginary parts are in $-4\pi^2/M^3$ and $4\pi^2/N^3$ respectively (with an $O(N^{-4}, M^{-4})$ error), by (8). Therefore, the ratio does lie above the real line, and the “pinched” angles of the limiting (grey) triangles in Figure 11 are both roughly

$$2\pi^2(N^{-3} + M^{-3})$$

radians. Very pinched, but not flat!

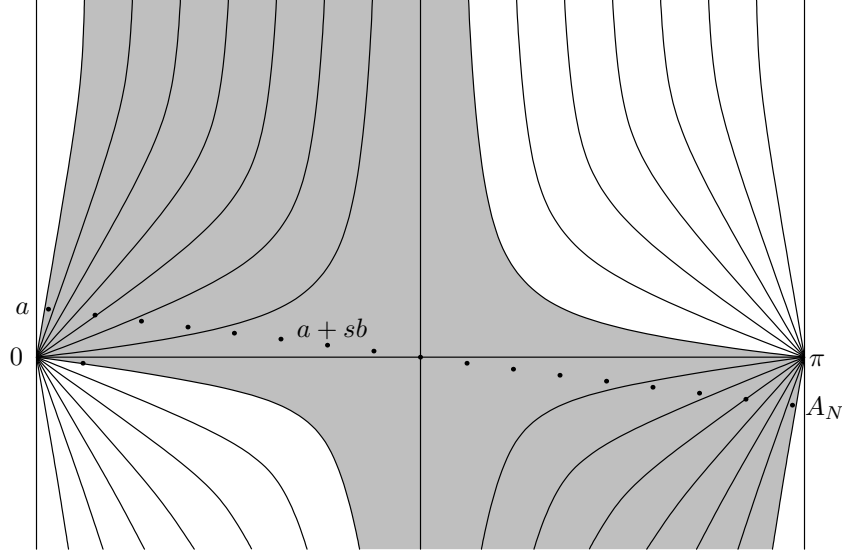


FIGURE 12. Level curves of $z \mapsto \arg(\sin z)$.

To check that $\arg(\frac{\sin A_s}{\sin b})$ lies in $(0, \pi/2)$ for all other $0 \leq s \leq N$, we need to draw the level curves of $z \mapsto \arg(\sin z)$ in \mathbb{C} . This is done in Figure 12, for $0 \leq \operatorname{Re}(z) \leq \pi$: the curves fall into 4 symmetric families (“quadrants” meeting at $\pi/2 \in \mathbb{C}$), and it is an easy exercise to check that the families above (resp. below) the real axis are made of convex (resp. concave) curves. The authorized region for the $A_s = a + sb$ is in grey (with a narrow collar near $\pi/2$); the forbidden regions are left in white. The segment $[A_0 A_N]$ clearly stays in the grey region, which implies the result.

By the same argument, the triangles in the fan of L^M are well-oriented, too. Therefore we may tile the plane with parallelograms (or fans) congruent to those in Figure 11 to get a Euclidean realization of Figure 4. \square

Finally, notice that the Kleinian group associated to the embedding of the left fan in Figure 11 contains the Möbius transformation $z \mapsto \frac{z \cos b - \sin b}{z \sin b + \cos b}$ (it sends each tetrahedron sitting above a triangle in the left half of the fan to the tetrahedron sitting above the similar triangle in the right half). Therefore, $2ib$ (and similarly $-2ib'$) are the complex lengths of very short closed geodesics in the hyperbolic manifold V_φ .

11. ONCE-PUNCTURED TORI AND 4-TIMES-PUNCTURED SPHERES

Theorem 1 is still true if we replace the once-punctured torus T by the four-times-punctured sphere S , and the map $\varphi : T \rightarrow T$ by an orientation-preserving homeomorphism $\varphi_S : S \rightarrow S$ (of course, we must specify how the “eigenvalues” of φ_S are defined). In fact, the tetrahedra of the resulting manifold V_{φ_S} and of V_φ are metrically the same; only the combinatorics of their gluing changes a little.

Define $R := \mathbb{R}^2 \setminus \mathbb{Z}^2$ and the maps $\alpha, \beta, \sigma : R \rightarrow R$ characterized by $\alpha(x) = x + (1, 0)$; $\beta(x) = x + (0, 1)$; $\sigma(x) = -x$. Then we have natural identifications

$T = R/\langle \alpha, \beta \rangle$ and $S = R/\langle \alpha^2, \beta^2, \sigma \rangle$. Define also $T' := R/\langle \alpha^2, \beta^2 \rangle$ (note that T' is a four-times-punctured torus).

It is easy to see that up to isotopy, any orientation-preserving diffeomorphism φ_S of S lifts to a map $\varphi_R : R \rightarrow R$ such that $\varphi_R(x) = Mx + v$ for some $M \in SL_2(\mathbb{Z})$ and $v \in \mathbb{Z}^2$. Moreover, $(\pm M)$ and $(v \bmod 2\mathbb{Z}^2)$ are unique. So we may define the eigenvalues of φ_S (up to sign) as those of M . Observe finally that φ_R induces orientation-preserving diffeomorphisms $\varphi' : T' \rightarrow T'$ and $\varphi_T : T \rightarrow T$.

There are obvious coverings $T' \rightarrow T$ and $T' \rightarrow S$, of degrees 4 and 2 respectively. Given an ideal triangulation τ_T of T (corresponding to a Farey triangle), we can lift τ_T to an ideal triangulation τ' of T' . Observe that σ acts on T' as a properly discontinuous involution fixing τ' , hence τ' descends to a triangulation τ_S of S . It is easy to see that τ_S has the combinatorics of a tetrahedron. If τ_T and τ_T^1 are separated by a diagonal exchange (see Subsection 3.1 for a definition), then τ_S and the corresponding τ_S^1 are separated by two diagonal exchanges on opposite edges. *Mutatis mutandis*, the construction of Section 3 provides ideal (topological) triangulations of $T' \times \mathbb{R}$ and $S \times \mathbb{R}$, as well as of their quotients $V_{\varphi'}$ and V_{φ_S} . There are coverings $V_{\varphi'} \rightarrow V_{\varphi_S}$ and $V_{\varphi'} \rightarrow V_{\varphi_T}$ (of degrees 2 and 4 respectively), and all these manifolds are hyperbolic when φ_S has distinct real eigenvalues.

* * *

APPENDIX A. GEOMETRIC TRIANGULATIONS OF TWO-BRIDGE LINK COMPLEMENTS

By David Futer

This appendix applies Guéritaud's techniques to find geometric triangulations for the hyperbolic two-bridge knot and link complements. The ideal triangulations in question were constructed and studied in great detail by Sakuma and Weeks [SW]. They are, in essence, the monodromy triangulations of 4-punctured sphere bundles, closed off in a slightly different way.

We will begin by reviewing two-bridge links and these ideal triangulations. We will then explain how the methods of the preceding paper give linear angle structures for these triangulations and prove that the volume function is maximized in the interior of the space of angle structures.

A.1. Braids and two-bridge links. Let S be a 4-punctured sphere, visualized concretely as a square pillowcase with the corners removed. A 4-string braid between two pillowcases, one interior and one exterior, defines a so-called *product region* $S \times I$. We will restrict our attention to alternating braids in which the top right strand is free of crossings. (See Figure 13(a)).

The mapping class $\varphi : S \rightarrow S$ induced by this braid can be described by a word

$$\Omega := \begin{cases} R^{a_1} L^{a_2} \dots R^{a_n} & \text{or} & L^{a_1} R^{a_2} \dots L^{a_n} & \text{with odd } n, \text{ or} \\ R^{a_1} L^{a_2} \dots L^{a_n} & \text{or} & L^{a_1} R^{a_2} \dots R^{a_n} & \text{with even } n. \end{cases}$$

Here, R encodes a crossing on the bottom pair of strands, and L encodes a crossing on the left pair of strands, as in Figure 14. Each *syllable* of Ω (that is, each maximal subword R^{a_i} or L^{a_i}) corresponds to a *twist region* in which two strands of the braid wrap around each other a_i times. As we read Ω from left to right, we scan the crossings from the outside in. Note that, unlike the case of punctured

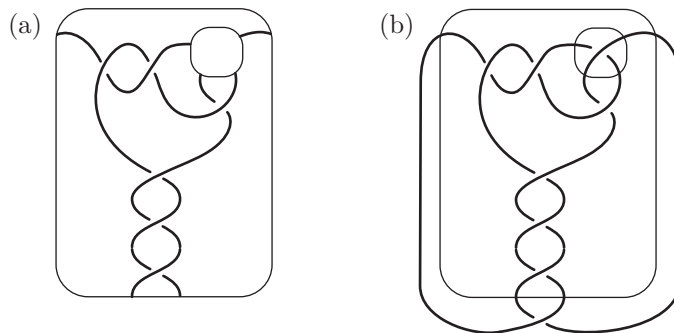


FIGURE 13. (a) An alternating braid between two pillowcases, described by the word $\Omega = R^3 L^2 R$. (b) The corresponding two-bridge link $K(\Omega)$.

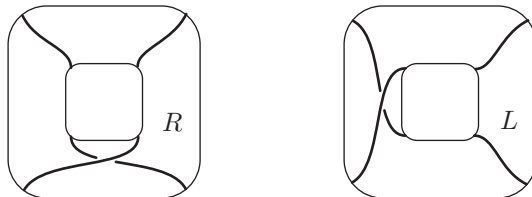


FIGURE 14. The letters R and L , acting on strands of a rational tangle.

torus bundles, our word Ω has a beginning and an end. For concreteness, we will focus on the case when Ω starts with R , as in Figure 1; the L -case is similar.

An alternating braid of this sort can be completed to a link diagram, as follows. Outside the outer pillowcase, we connect the bottom left strand to the top right, and the bottom right strand to the top left, adding an extra crossing. (Up to isotopy of S^2 , there is a unique way to do this while keeping an alternating projection. In Figure 13(b), the extra crossing was arbitrarily placed at the bottom of the diagram.) Similarly, inside the inner pillowcase we connect the strands in a diagonal fashion, adding an extra crossing. This creates an alternating link $K(\Omega)$, as in Figure 13(b).

K is called a *two-bridge link* because this diagram can be isotoped so that the pillowcases are horizontal, and the connecting strands form two bridges between the strands of the braid. It is well-known that, apart from the trivial link of one or two components, every two-bridge link can be constructed in this way. (See, for example, [Mu, Theorems 9.3.1 and 9.3.2].)

William Menasco's theorem about hyperbolic alternating links [Me] contains the following special case.

Theorem 19. *The two-bridge link $K(\Omega)$ is hyperbolic if and only if Ω has two or more syllables.*

Just as with punctured torus bundles, we will give a direct proof of the “if” direction of this theorem by finding a geometric ideal triangulation of the link

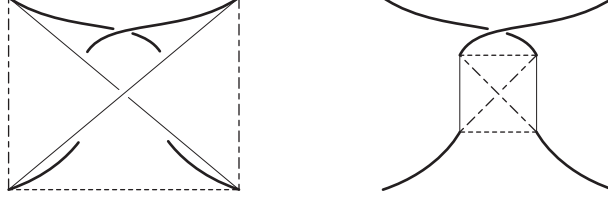


FIGURE 15. Two views of the same 4-punctured sphere S_i living near a crossing in the link diagram. In this figure, arcs with the same dashed pattern have the same slope on S_i .

complement. The “only if” direction is immediate: a word with a single syllable produces a link with a single twist region, which must be a torus link.

A.2. The ideal triangulation. The word Ω describes a monodromy triangulation of the product region $S \times I$, in exactly the same fashion as for punctured torus bundles. In fact, because this product region is the complement of a braid in S^3 , we can locate the edges of the triangulation concretely in the projection diagram.

Let $c = \sum_{i=1}^n a_i$ be the length of Ω . Each letter Ω_i ($1 \leq i \leq c$), and thus each crossing in the alternating braid, corresponds to a 4-punctured sphere $S_i \subset S^3 \setminus K$, with the four strands of K seen in Figure 14 passing through the four punctures. The braid induces an ideal triangulation on each S_i , whose edges come from arcs in the diagram that look vertical and horizontal immediately before and/or after the corresponding crossing. See Figure 15.

Just as with punctured torus bundles, we can locate the progressively changing triangulations in the Farey tessellation F . Each triangulation of a 4-punctured sphere S_i , containing six edges of three different slopes, corresponds to a Farey triangle t_i . Triangles t_i and t_{i+1} share an edge e_i , whose endpoints are the shared slopes of S_i and S_{i+1} . If $\Omega_i = R$, the path from e_{i-1} to e_i takes a right turn across t_i ; if $\Omega_i = L$, the path takes a left turn. This rule also defines an *initial edge* e_0 , because $\Omega_1 = R$, so a right turn should take e_0 to e_1 . Similarly, the action of Ω_c defines a *terminal edge* e_c .

For each e_i , $1 \leq i \leq c-1$, the 4-punctured spheres S_i and S_{i+1} are joined together along four edges, two for each endpoint of e_i . In between them lies a layer $\Delta_i = \Delta(e_i)$ of two tetrahedra, whose bottom surface S_i has the triangulation of t_i and whose top surface S_{i+1} has the triangulation of t_{i+1} . (See Figure 16 for an example). Stacking these tetrahedron layers together produces a layered triangulation of the product region between S_1 and S_c .

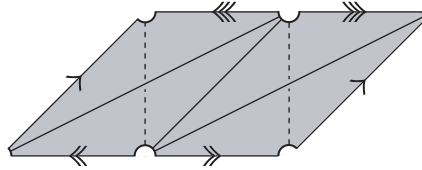


FIGURE 16. The tetrahedron layer $\Delta_1 = \Delta(e_1)$, made of two tetrahedra contained between 4-punctured spheres S_1 and S_2 . (Sides with identical arrows are identified.)

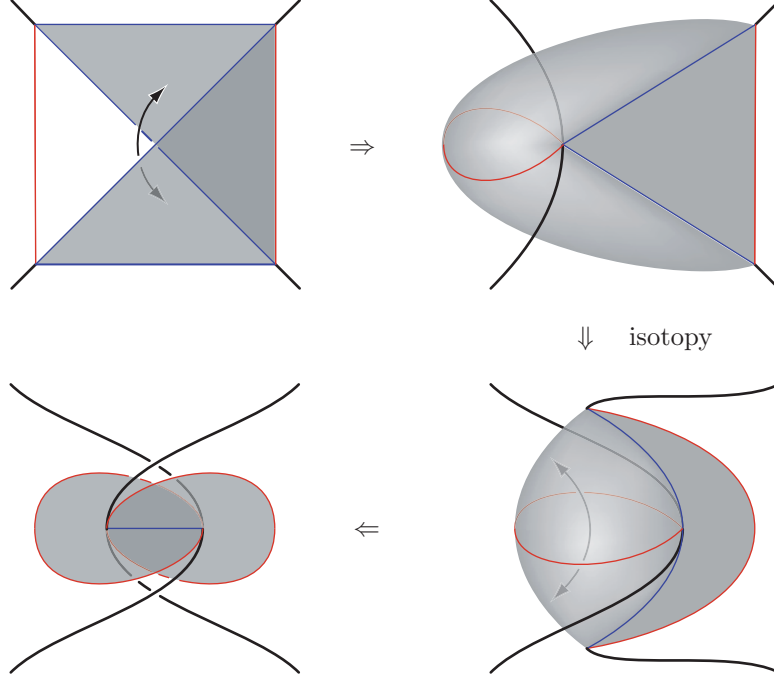


FIGURE 17. Folding the pleated surface S_1 produces the first two crossings in the link.

If we wanted to construct a bundle of 4-punctured spheres over the circle, we would glue the top of this product region to the bottom. To recover the complement of the link $K(\Omega)$, we follow a slightly different procedure. On the 4-punctured sphere S_1 , corresponding to the first crossing inside the outer pillowcase, let the *peripheral edges* be the edges whose slope is the vertex of t_1 opposite the initial edge e_0 .

We will fold S_1 along the two peripheral edges, identifying its ideal triangles in pairs. Figure 17 shows that this creates exactly the desired effect of connecting the strands of K in pairs, with a twist. This full twist corresponds to the first two crossings in the link projection: the first crossing in the braid, as well as the “extra” crossing outside the outer pillowcase. The four non-peripheral edges on S_1 are identified to a single edge, isotopic to a short arc near the crossing. The two ideal triangles that remain after folding are clasped together around this edge, which we call the *core* of the clasp.

Let α be the mirror image of the peripheral slope across e_0 in the Farey graph. Topologically, folding S_1 as above amounts to attaching a thickened disk of boundary slope α to the outer pillowcase [SW, Lemma II.2.5].

In a similar fashion, we define the peripheral edges on S_c to be the edges whose slope is the vertex of t_c opposite e_c . We fold S_c along these two peripheral edges, identifying its faces to a clasp of two ideal triangles. Topologically, attaching 2-handles to S_1 and S_c results in a space homeomorphic to the link complement. Combinatorially, folding S_1 and S_c defines a gluing pattern for all the faces of the tetrahedra, giving us an ideal triangulation of $S^3 \setminus K$. See [SW, Section II.2] for more details of this triangulation.

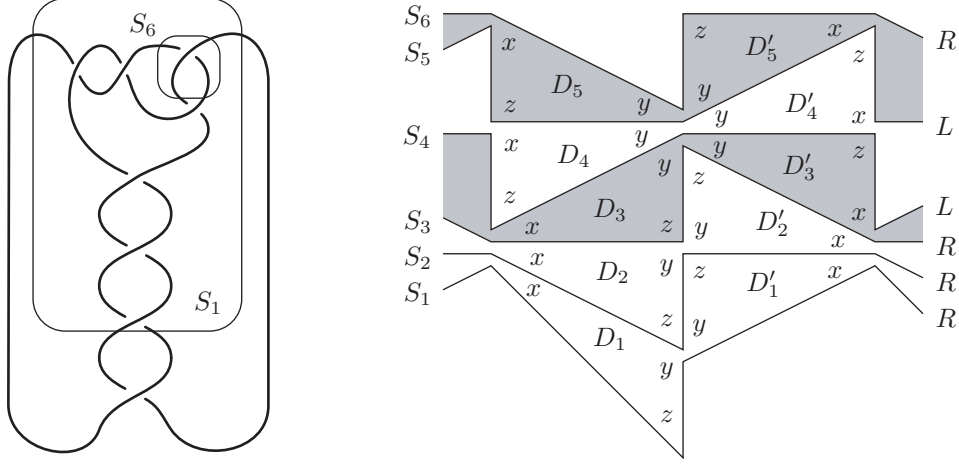


FIGURE 18. Left: the link $K(\Omega)$ corresponding to $\Omega = R^3 L^2 R$. Right: a cusp view of the product region between S_1 and S_c .

A.3. Combinatorics at the cusp. To describe the combinatorics of the boundary component(s) of $S^3 \setminus K$, we will first focus on the product region between the pleated surfaces S_1 and S_c . In the layered triangulation of this product region, each layer Δ_i consists of two tetrahedra, D_i and D'_i , as in Figure 16. It is clear from the figure that each tetrahedron has exactly one vertex at each puncture of S_i , i.e. at each strand of the 4-string braid between S_1 and S_c . Since the combinatorics of the four strands are identical, let us focus on a single puncture of the 4-punctured sphere.

The tetrahedron layer Δ_i intersects the neighborhood of a puncture in two *boundary triangles*, one from a truncated vertex of D_i and one from D'_i . These boundary triangles meet at two vertices that come from shared edges of D_i and D'_i . (This completes a loop, corresponding to the meridian of a component of K). The apices of the two triangles point in different directions, as in Figure 3 on page 6. As with punctured torus bundles, these layers of boundary triangles are stacked together, forming fans that correspond to syllables of the word Ω .

The resulting cusp triangulation, corresponding to the product region of the link $K(R^3 L^2 R)$, is shown in Figure 18. As in Figure 4, the triangles are shown opened up, and the hinge layers are shaded. Observe that the picture is combinatorially equivalent to the quotient of a punctured torus bundle cusp by the hyperelliptic involution.

We have labeled the dihedral angles of the tetrahedra of Δ_i by dihedral angles x_i, y_i, z_i , following the same conventions as in Figure 4. Note that our choices of dihedral angles force the tetrahedra D_i and D'_i to be isometric; this does not impede the goal of finding a geometric triangulation. In the sequel, we will not distinguish between D_i and D'_i .

When the pleated surface S_1 is folded to form a clasp, the zigzag line in which it intersects the cusp also becomes folded, creating a “hairpin turn”. Because this folding procedure joins the punctures of S_1 in pairs, as in Figure 17, the boundary triangles on those punctures are also joined together. The resulting cusp

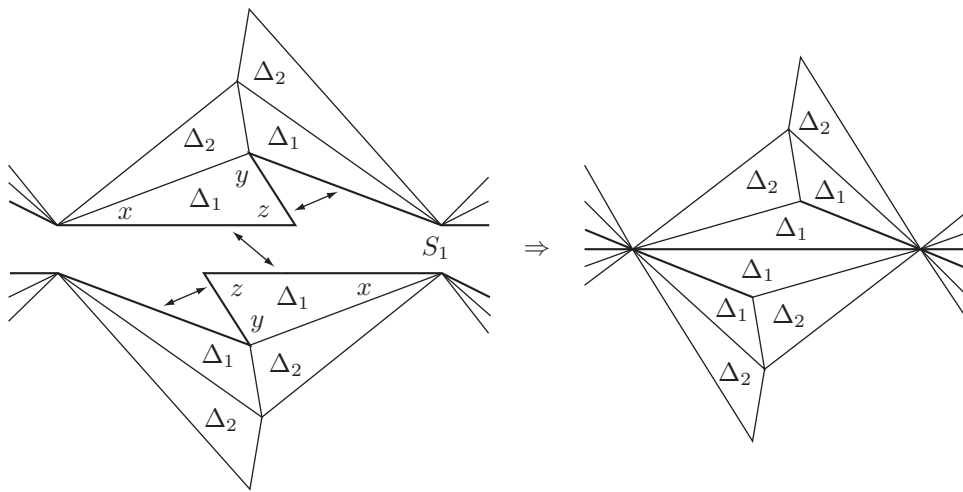


FIGURE 19. A cusp view of the folding that occurs at a clasp.

triangulation in the neighborhood of S_1 can be seen in Figure 19. At the other end of the product region, the clasp of S_c appears on the cusp in the same way.

Once we have folded the clasp surfaces as prescribed, the truncated vertices of the tetrahedra combine to form either a single torus that traverses the product region four times (in case K is a knot), or two tori, each of which traverses the product region twice (in case K is a two-component link). In either case, the local combinatorics are the same, and the affine equations that the dihedral angles of the tetrahedra must satisfy are derived in the same way.

To find the hyperbolic structure on $S^3 \setminus K$, we will study the space P of *angle structures* for the triangulation, i.e. the space of positive dihedral angles that line up correctly around each edge. We need to complete three steps:

- (1) Parametrize P and check that it is non-empty, as in Section 5.
- (2) Show that a critical point of the volume functional on P gives a complete hyperbolic metric, as in Section 6.
- (3) Prove that at any point on the boundary of \overline{P} , the volume can be increased by un-flattening the flat tetrahedra, as in Sections 7–9.

This will imply that the volume functional is maximized in the interior of P , guaranteeing a critical point and thus a hyperbolic metric. For each of the three steps, the argument is essentially the same as Guéritaud's.

A.4. Angle structures and volume. Following Section 5 of the main article, we will parametrize the dihedral angles of the tetrahedra by *pleating angles* on the pleated 4-punctured spheres. Each sphere S_i described above has a natural transverse orientation that points (equivalently) toward the inside of the link projection, toward increasing indices, and upward in Figure 18. Just as in Section 5, for any edge $e \subset S_i$, we can define the *pleating angle* α to be the (signed) external angle at e , with signs chosen so that α is positive whenever the angle above e is less than π .

On the pleated sphere S_{i+1} living between Δ_i and Δ_{i+1} , this definition will give pleating angles

$$-2w_i, \quad 2w_{i+1}, \quad \text{and} \quad 2w_i - 2w_{i+1},$$

exactly as in (2). The clasp surface S_1 , which borders Δ_1 on one side and is folded on the other side, will have pleating angles $-\pi$, $2w_1$, and $\pi - 2w_1$, where the pleating angle of $-\pi$ corresponds to the hairpin turn in Figure 19. Thus, if we define $w_0 = \pi/2$ (even though there is no tetrahedron layer Δ_0), the pleating angles on S_1 will be given by the same expressions as above. Similarly, setting $w_c = \pi/2$ allows us to label the pleating angles on S_c by the same expressions as in (2).

Lemma 20. *For $i = 0, \dots, c$, choose a parameter w_i , such that $w_0 = w_c = \pi/2$ and w_1, \dots, w_{c-1} satisfy the range, concavity, and hinge conditions (4). For each such choice of parameters, set the dihedral angles of the tetrahedra as in Table 3. Then*

- (1) *for each Δ_i , the angles x_i, y_i, z_i are positive and add up to π ,*
- (2) *the dihedral angles around each edge add up to 2π , and*
- (3) *for each S_i , the pleating angles add up to 0.*

Proof. The range, concavity, and hinge conditions imply that all the tetrahedron angles x_i, y_i, z_i are positive, and the claim that their sum is π is immediate from Table 3. For each pleated surface S_i , the pleating angles sum to 0 by construction. Therefore, it remains to check the angle sum around each edge e of $S^3 \setminus K$.

If e is not the core of S_1 or S_c , the combinatorial picture of Figure 18 is the same as the one for torus bundles. Thus, as in Section 5, each layer Δ_i contributes precisely the difference between the pleating angles of the neighboring surfaces, and the sum around e simplifies to 2π . If e is the core of a clasp, say the core of S_1 , the left panel of Figure 19 shows that four sectors contribute dihedral angles at e : two sectors that have angle z_1 , plus two fans of angles above pleated surface S_1 , each having dihedral angle $2w_1$. Thus, because $z_1 + 2w_1 = \pi$, the total angle sum at e is 2π . \square

By Lemma 20, our triangulation will have an angle structure whenever we set $w_0 = w_c = \pi/2$ and interpolate between these parameters in a way that satisfies the range, concavity, and hinge conditions. One can always do this graphically, by first fixing w_i for the hinge indices and then connecting the hinges by pieces of parabolas, as in Figure 6 (this is where we use the hypothesis that Ω contains at least one hinge).

Lemma 21. *Let P be the open affine polyhedron of angle structures for the triangulation of $S^3 \setminus K$, parametrized as in Lemma 20 by sequences $(\frac{\pi}{2}, w_1, \dots, w_{c-1}, \frac{\pi}{2})$. Then a point of P is a critical point of the volume functional \mathcal{V} if and only if the corresponding tetrahedron shapes give a complete hyperbolic structure on $S^3 \setminus K$.*

Just like Lemma 4, this is an instance of a much more general theorem of Rivin, Chan, and Hodgson [CH, Ri]. It is also possible to prove Lemma 21 directly, using the same line of argument as in Lemma 4, although in the setting of two-bridge links this would require considering a number of special cases.

A.5. Flat tetrahedra never maximize volume. The proof that the maximum of \mathcal{V} occurs in the interior of P closely tracks Sections 7-9 of Guéritaud's paper. We begin by ruling out many types of degeneracies on ∂P .

Lemma 22. *Let (w_1, \dots, w_{c-1}) be the point of \overline{P} at which the volume functional \mathcal{V} attains its maximum. Then (w_i) has the following properties:*

- (1) *For each i , if one of x_i, y_i, z_i is 0, then two of them are 0, i.e. Δ_i is flat.*
- (2) *If Δ_i is flat, then $w_i = 0$.*
- (3) *If Δ_i is flat, then i is a hinge index, not equal to 1 or $c - 1$.*
- (4) *If Δ_i is flat, then i is adjacent to at least two consecutive identical letters.*
- (5) *If both hinge layers at the ends of a syllable R^k or L^k are flat, then $k \geq 3$.*

Proof. All the discussion and results of Section 7 apply equally well in our context. Thus we have conclusion (1) as a restatement of Proposition 11. The domino effect of Proposition 12 also applies; in fact, it is clear from the proof of the Proposition that the domino effect works both forward and backward. Thus it does not matter that our word Ω is not cyclic.

Almost all the claims of (2)–(5) are proved in Section 7, either in Proposition 13 or in the discussion that follows. The one exception is the claim that Δ_1 and Δ_{c-1} cannot flatten. This follows because, in the case of two-bridge links, $w_0 = w_c = \pi/2$. Thus setting w_1 or w_{c-1} to 0 or $\pi/2$ will trigger the domino effect and force all the tetrahedra to flatten, giving a volume of 0. \square

It remains to prove that at any point $(w_i) \in \partial \overline{P}$ satisfying the properties of Lemma 22, the volume will increase as we move into the interior of P . Following Guéritaud, we do this using the geometrical statement of Lemma 16. The proof of this lemma transfers perfectly to our context when the fan under consideration corresponds to a subword in the interior of Ω . As it turns out, the same statement is even easier to prove when the degenerate layer is near the beginning or end of Ω .

Lemma 23. *Recall the word $\Omega = R^{a_1} L^{a_2} \dots$, and suppose that the hinge layer Δ_{a_1} has flattened, with $w_{a_1} = 0$. Then the fan corresponding to $R^{a_1} L$ admits a complete Euclidean structure with boundary along S_{a_1} . Let Q, P, T be the lengths of the segments of the broken line in which S_{a_1} intersects the cusp, as in Figure 20. Then $Q < P + T$.*

Of course, the analogous statement holds near the end of Ω .

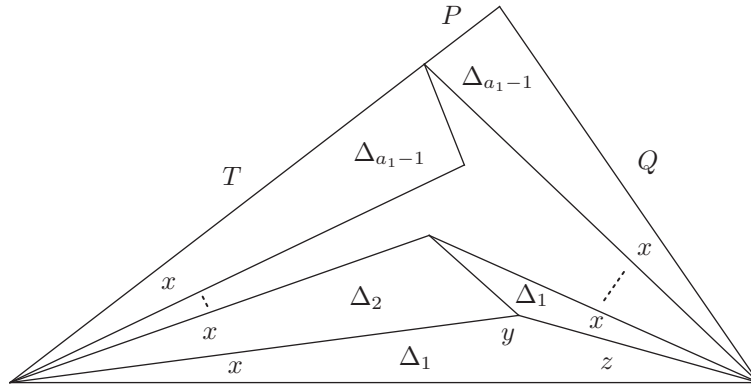


FIGURE 20. In a fan at the beginning of Ω , $Q < P + T$.

Proof. Note that, by Lemma 22, we have $a_1 \geq 2$. For all $1 \leq i \leq a_1 - 2$, the parameter w_i can vary in a small interval, and no generality is lost in assuming that $\partial\mathcal{V}/\partial w_i = 0$. (Otherwise, volume is easy to increase). Then, as in the proof of Lemma 16, the criticality of volume with respect to these parameters implies that the fan of $R^{a_1}L$ has a complete Euclidean structure. If $i > 1$, the computation is the same as in Sublemma 6. If $i = 1$, the angle z_0 of Figure 7 is replaced by the hairpin turn, and the factor $\frac{\sin y_0}{\sin x_0}$ disappears from the computation of $\exp(-\partial\mathcal{V}/\partial w_1)$. Thus we once again have $1 = \exp(-\partial\mathcal{V}/\partial w_1) = |\psi(\alpha)|$, where ψ is the reduced holonomy and α is a loop around the vertex at the hairpin turn.

In our situation, the fan of $R^{a_1}L$ is a (tessellated) Euclidean triangle, as in Figure 20, in which Q and $P+T$ are two of the sidelengths. In the triangular fan, the angle opposite Q is $x_1 + \dots + x_{a_1-1}$, while the angle opposite $P+T$ is $z_1 + x_1 + \dots + x_{a_1-1}$. Thus, because its side is opposite the smaller angle, $Q < P+T$. \square

Armed with Lemma 16 and its analogue in Lemma 23, we can complete the proof of Theorem 19 by following the argument of Section 9. For each hinge index j with $w_j = 0$, we pick a vector along which to deform the neighboring parameters, in a way that will maximize the derivative of volume. Deforming in this optimal direction with speed ε , we can compute $\partial\mathcal{V}/\partial\varepsilon$ in terms of the geometry of the fan(s) that adjoin Δ_j .

In most situations, the exponentiated derivative appears as a product of the exact same sine ratios as in Section 9. The only exception occurs when $j = 2$ or $j = c - 2$, because there are no tetrahedra corresponding to w_0 or w_c . If (without loss of generality) $j = 2$, the angle z_0 is replaced by the hairpin turn, while the factor $\frac{\sin y_0}{\sin x_0}$ disappears from the computation of P/T , just as in the proof of Lemma 23. Thus $\partial\mathcal{V}/\partial\varepsilon$ has the same expression in terms of Q, Q', P, P', T, T' as in Section 9.

In every case, the geometric statement $Q < P+T$, applied to two fans if necessary, implies that $\partial\mathcal{V}/\partial\varepsilon > 0$. Therefore \mathcal{V} is maximized at a critical point where all tetrahedron angles are positive, completing the proof of Theorem 19.

REFERENCES

- [AH] Pekka Alestalo, Heinz Helling, *On torus fibrations over the circle*, Sonderforschungsbereich SFB-343, preprint 97-005, Bielefeld.
- [ASWY] Hirotaka Akiyoshi, Makoto Sakuma, Masaaki Wada, Yasushi Yamashita, *Jørgensen's picture of punctured torus groups and its refinement*, in *Kleinian Groups and Hyperbolic 3-Manifolds*, Y. Komori, V. Markovic, C. Series (Ed.), Lond. Math. Soc. Lecture Notes, **299**, Cambridge Univ. Press, 2003.
- [CH] Ken Chan, *Constructing hyperbolic 3-manifolds*, Undergraduate thesis with Craig Hodgson, University of Melbourne, 2002.
- [Co] Yves Colin de Verdière, *Un principe variationnel pour les empilements de cercles*, Inventiones Math. **104** (1991) 655–669.
- [Gu] François Guéritaud, *Quasifuchsian punctured-torus groups with given bending data*, in preparation.
- [He] Heinz Helling, *The trace fields of a series of hyperbolic manifolds*, SFB-343, Preprint 99-072, Bielefeld.
- [Ko] Tino Koch, *Fordsche Fundamentalbereiche hyperbolischer einfach-punktierter Torus-Bündel*, SFB-343, Preprint 99-009, Bielefeld.
- [La] Marc Lackenby, *The canonical decomposition of once-punctured torus bundles*, Comment. Math. Helv. **78** (2003) 363–384.
- [Me] William Menasco, *Closed incompressible surfaces in alternating knot and link complements*, Topology **23** (1984), no. 1, 37–44.

- [Mi] John Milnor, *Hyperbolic geometry: the first 150 years*, Bull. Amer. Math. Soc. **6** (1982), no. 1, 9–24.
- [Mu] Kunio Murasugi, *Knot theory and its applications*, Birkhäuser Boston Inc., Boston, MA, 1996 (translated from the 1993 Japanese original by Bohdan Kurpita).
- [NZ] Walter Neumann and Don Zagier, *Volume of hyperbolic 3-manifolds*, Topology **24** (1985) 307–332.
- [Ot] Jean-Pierre Otal, *Le théorème d'hyperbolisation pour les variétés fibrées de dimension 3*, Astérisque **235** (1996), SMF.
- [Ri] Igor Rivin, *Euclidean structures on simplicial surfaces and hyperbolic volume*, Ann. of Math. **139** (1994) 553–580.
- [SW] Makoto Sakuma and Jeffrey Weeks, *Examples of canonical decompositions of hyperbolic link complements*, Japan. J. Math. (N.S.) **21** (1995), no. 2, 393–439.

FRANÇOIS GUÉRITAUD, DMA – UMR 8553 (CNRS), ÉCOLE NORMALE SUPÉRIEURE, 45 RUE D'ULM, 75005 PARIS, FRANCE

E-mail address: `Francois.Gueritaud@ens.fr`

DAVID FUTER, MATHEMATICS DEPARTMENT, MICHIGAN STATE UNIVERSITY, EAST LANSING, MI 48824, USA

E-mail address: `dfuter@math.msu.edu`